Reactive Rigid-Rod Organometallic Polymers Involving Linear Triplatinum Units Connected by π-Conjugated Bisisocyanides

Tomoaki Tanase,*,† Eri Goto,† Rowshan A. Begum,† Makiko Hamaguchi,† Shuzhong Zhan,† Masayasu Iida,† and Ken Sakai‡

Department of Chemistry, Faculty of Science, Nara Women's University, Kitauoya-higashi-machi, Nara 630-8285, Japan, and Department of Applied Chemistry, Faculty of Engineering, Tokyo University of Science, Kagurazaka 1-3, Shinjuku-ku, Tokyo 162-8601, Japan

Received July 19, 2004

Axial ligand exchange reactions of $[Pt_3(\mu\text{-dpmp})_2(XylNC)_2](PF_6)_2$ (**1**) with monoisocyanide molecules afforded a series of linear triplatinum complexes, $[Pt_3(\mu\text{-dpmp})_2(RNC)_2](PF_6)_2$ (R = 2,4,6-mesityl (**2**), *tert*-butyl (**4**), 4-tolyl (**5**)) and $[Pt_3(\mu\text{-dpmp})_2(XylNC)(t\text{-BuNC})](PF_6)_2$ (**3**), which were characterized by spectroscopic, X-ray crystallographic, and absorption (EXAFS) analyses. With the increase of π-acidity of the terminal isocyanide, the Pt−Pt bond length became longer due to electron transfer from the Pt_3 core to the isocyanide group. Terminal ligand exchange reactions of **1** with bulky aromatic bisisocyanides (bisNC*n*) led to successful isolation of the rigid-rod triplatinum cluster polymers formulated as $\{[Pt_3(\mu\text{-dpmp})_2(bisNCn)](PF_6)_2\}_n$ (bisNC*n* = 2,3,5,6-tetramethylphenylene-1,4-bisisocyanide (bisNC1) (**7a**), 3,3′,5,5′-tetramethylbisphenylene-4,4′-bisisocyanide (bisNC2) (**7b**)). The structure of compound **7a**, determined by X-ray crystallography, was composed of the linear, metal−metal bonded $\{Pt_3(\mu\text{-dpmp})_2\}^{2+}$ fragments (av Pt−Pt = 2.699 Å) covalently connected by the bisisocyanide molecules, resulting in an infinite rigid-rod polymeric structure. By using less bulky bisisocyanides, the ligand exchange reaction stopped at the formation of the triplatinum cluster dimers $[(bisNCn)Pt_3(\mu\text{-dpmp})_2(bisNCn)Pt_3(\mu\text{-dpmp})_2(bisNCn)](PF_6)_4$ (bisNC*n* = phenylene-1,4-bisisocyanide (bisNC3) (**8a**), 2,5-dimethylphenylene-1,4-bisisocyanide (bisNC4) (**8b**)), which were characterized by EXAFS analyses to involve the weakly metal−metal bonded Pt_3 fragments (av Pt−Pt = 2.85 Å). The rigid-rod polymer **7a** was demonstrated to be quite reactive even in heterogeneous systems toward H^+, NO^+, tetracyanoethylene (tcne), and electron-deficient alkynes, to afford the cluster polymers formulated as $\{[Pt_3(\mu\text{-H})(\mu\text{-dpmp})_2(bisNC1)](BF_4)_3\}_n$ (**13**), $\{[Pt_3(\mu\text{-NO})_2(\mu\text{-dpmp})_2(bisNC1)](BF_4)_4\}_n$ (**14**), $\{[Pt_3(\mu\text{-}C_{12}N_8)(\mu\text{-dpmp})_2(bisNC1)](PF_6)_2\}_n$ (**15**), and $\{[Pt_3(\mu\text{-}R^1C_2R^2)(\mu\text{-dpmp})_2(bisNC1)](PF_6)_2\}_n$ (**16a**, R^1 = H, $R^2 = CO_2CH_3$; **16b**, $R^1 = R^2 = CO_2CH_3$). The structures of the polymers **13**−**16** were estimated on the basis of the X-ray crystallographic and spectroscopic analyses for the related reference complexes $[Pt_3(\mu\text{-H})(\mu\text{-dpmp})_2(XylNC)_2]^{3+}$ (**9**), $[Pt_3(\mu\text{-NO})_2(\mu\text{-dpmp})_2(RNC)_2](BF_4)_4$ (**10**, R = Xyl, Mes), $[Pt_3(\mu\text{-}C_{12}N_8)(\mu\text{-dpmp})_2(RNC)_2](PF_6)_2$ (**11**, R = Xyl, Mes), and $[Pt_3(\mu\text{-}R^1C_2R^2)(\mu\text{-dpmp})_2(XylNC)_2](PF_6)_2$ (**12**, R^1 = H or $COOCH_3$, $R^2 = COOCH_3$).

Introduction

Ordered assemblies of metal−metal bonded transition metal clusters with organic linkers have attracted increasing attention since they have the potential to act as molecular-based multifunctional devices. Rigid-rod polymers containing mononuclear transition metal fragments connected by linear π-conjugated organic linkers, such as bisacetylide and bisisocyanide, have been extensively studied in regard to their photochemical and optical properties.[1] However, such polymers with metal−metal bonded di- and multimetallic units have rarely been investigated, despite that a variety of functions and reactivities with multimetallic systems can be introduced into the materials.[2] Examples of rigid-rod cluster polymers have been limited only to the oligomers of di- and triplatinum units $\{Pt_2(\mu\text{-dppm})_2\}^{2+}$ and $\{Pt_3(\mu\text{-dppm})_3\}^{2+}$ (dppm = bis(diphenylphosphino)methane), connected by phenylene-1,4-bisacetylide and phenylene-1,4-bisisocyanide,[3] which were not investigated in detail owing to their poor solubility. Most efforts along this line have resulted in the characterization of di- and trimers of di- and multinuclear metal fragments connected by π-conjugated organic linkers.[4] We have stud-

* To whom correspondence should be addressed. E-mail: tanase@cc.nara-wu.ac.jp.
† Nara Women's University.
‡ Tokyo University of Science.

(1) (a) Hagiwara, N.; Sonogashira, K.; Takahashi, S. *Adv. Polym. Sci.* **1984**, *41*, 149. (b) Lavastre, O.; Even, M.; Dixneuf, P. H.; Pacreau, A.; Varion, J. P. *Organometallics* **1996**, *15*, 184. (c) Puddephatt, R. J. *Chem. Commun.* **1998**, 1055. (d) Manners, I. *Chem. Commun.* **1999**, 857.

(2) (a) Adams, D. A., Cotton, F. A., Eds. *Catalysis by Di- and Polynuclear Metal Cluster Complexes*; Wiley-VCH: New York, 1998. (b) Balch, A. L. In *Progress in Inorganic Chemistry*; Lippard, S. J., Ed.; Wiley: New York, 1994; Vol. 41, p 239. (c) Balch, A. L. In *Homogeneous Catalysis with Metal Phosphine Complexes*; Pignolet, L. H., Ed.; Plenum Press: New York, 1983; p 167.

10.1021/om0494566 CCC: $27.50
Publication on Web 11/03/2004

ied the synthesis and characterization of homo- and heterometallic di- and trinuclear Pt and Pd complexes supported by a tridentate phosphine ligand, bis(diphenylphosphinomethyl)phenylphosphine (dpmp).[5] During our studies, the linearly ordered triplatinum cluster, $[Pt_3(\mu\text{-dpmp})_2(XylNC)_2](PF_6)_2$ (**1**), has been prepared by site-selective incorporation of Pt^0 atom into the dpmp-bridged diplatinum complex $[Pt_2(\mu\text{-dpmp})_2(XylNC)_2](PF_6)_2$ (XylNC = 2,6-xylyl isocyanide).[5e] Complex **1** possesses a widespread, coordinatively unsaturated plane comprised of the three platinum atoms with 44 valence electrons and is, thus, of general interest as a simple model for the interactions of metal surfaces with small organic molecules. In the present study, using complex **1** as starting material, rigid-rod organometallic polymers including the linear triplatinum units, $\{Pt_3(\mu\text{-dpmp})_2\}^{2+}$, connected by π-conjugated bisisocyanides have successfully been synthesized, utilizing its axial isocyanide ligand exchange reactions. The triplatinum units of the polymer were revealed to be very reactive with small molecules and ions, such as H^+, NO^+, tetracyanoehtylene (tcne), and electron-deficient alkynes, even in heterogeneous systems. We wish to report herein the full details of the reactive rigid-rod organometallic polymers involving the linear triplatinum units together with the related triplatinum complexes obtained from complex **1**. Preliminary results concerning $[Pt_3(\mu\text{-NO})_2(\mu\text{-dpmp})_2(RNC)_2](BF_4)_4$ (**10**) and $[Pt_3(\mu\text{-}C_{12}N_8)(\mu\text{-dpmp})_2(RNC)_2](PF_6)_2$ (**11**) have already been communicated.[5c,d]

Experimental Section

Solvents were dried and freshly distilled prior to use. Other reagents were of commercial grade and were used as received. $[Pt_3(dpmp)_2(XylNC)_2](PF_6)_2\cdot(CH_3)_2CO$ (**1**) was prepared by the method already reported.[5e] $[Pt_3(\mu\text{-H})(\mu\text{-dpmp})_2(XylNC)_2](PF_6)_3$ (**9b**) was prepared by a procedure similar to that for $[Pt_3(\mu\text{-H})(\mu\text{-dpmp})_2(XylNC)_2](BF_4)_3$.[5k] Phenylene-1,4-bisisocyanide (bisNC3) was purchased from Aldrich. 2,3,5,6-tetramethylphenylene-1,4-bisisocyanide (bisNC1), 3,3′,5,5′-tetramethylbiphenylene-4,4′-bisisocyanide (bisNC2), and 2,5-dimethylphenylene-1,4-bisisocyanide (bisNC4) were prepared by known methods.[6] All reactions were carried out under a nitrogen atmosphere with standard Schlenk and vacuum line techniques.

Measurement. ^1H NMR spectra were measured on a Varian Gemini 2000 instrument at 300 MHz. Chemical shifts were calibrated to tetramethylsilane as an external reference. $^{31}P\{^1H\}$ NMR spectra were recorded on the same instrument at 121 MHz, with chemical shifts being calibrated to 85% H_3PO_4 as an external reference. Infrared and electronic absorption spectra were recorded with Shimadzu UV3000 and Jasco FT/IR-410 spectrometers, respectively. Electrochemical measurements were performed with a HOKUTO-Denko HZ-3000 system on ca. 1 mM acetonitrile solutions of the samples (**1**, **2**, **4**, **5**, and **7a**) containing 0.1 M $[n\text{-}Bu_4N][PF_6]$ as supporting electrolyte and by using a standard three-electrode cell consisting of a $Ag/AgPF_6$ reference electrode, platinum wire as the counter-electrode, and glassy carbon as the working electrode. Controlled potential electrolysis was performed with the same instrument using a mercury pool working electrode.

Preparation of $[Pt_3(\mu\text{-dpmp})_2(MesNC)_2](PF_6)_2$ (2). To an acetone solution (30 mL) containing $[Pt_3(dpmp)_2(XylNC)_2](PF_6)_2\cdot(CH_3)_2CO$ (**1**) (211 mg, 0.096 mmol) was added mesityl isocyanide (MesNC) (206 mg, 1.4 mmol). The solution was stirred at room temperature for 12 h. The solvent was removed under reduced pressure, and the residue was thoroughly washed with diethyl ether. The residue was extracted with dichloromethane (10 mL), which was concentrated to ca. 2 mL. After careful addition of diethyl ether (ca. 4 mL), the solution was allowed to stand at 2 °C to afford reddish orange crystals of $[Pt_3(\mu\text{-dpmp})_2(MesNC)_2](PF_6)_2$ (**2**), which were separated by filtration, washed with diethyl ether, and dried in vacuo (171 mg, yield 82%). Anal. Calcd for $C_{84}H_{80}N_2P_8F_{12}Pt_3$: C, 46.31; H, 3.70; N, 1.29. Found: C, 45.98; H, 3.71; N, 1.28. IR (Nujol): 2139 (N≡C), 838 (PF_6) cm^{-1}. UV−vis (in CH_2Cl_2): λ_{max} (log ϵ) 499 (2.79), 389 (4.13), 360 (4.04), 297 (3.95) nm. ^1H NMR (in CD_2Cl_2): δ 1.38 (s, *o*-Me, 12H), 2.10 (s, *p*-Me, 6H), 4.8−5.4 (m, CH_2, 8H), 6.8−8.2 (m, Ar, 54H). $^{31}P\{^1H\}$ NMR (in acetone-d_6): δ −15.9 (m, 2P, $^1J_{PtP}$ = 2793 Hz), 2.0 (m, 4P, $^1J_{PtP}$ = 2976 Hz). Recrystallization of **2** from an acetone/diethyl ether mixed solvent afforded block-shaped crystals of **2**·2{$(CH_3)_2CO$}, which were suitable for X-ray crystallography.

Preparation of $[Pt_3(\mu\text{-dpmp})_2(t\text{-BuNC})(XylNC)](PF_6)_2$ (3). To a dichloromethane solution (20 mL) containing **1** (105 mg, 0.048 mmol) was added a 0.20 M benzene solution of *tert*-butyl isocyanide (*t*-BuNC) (0.40 mmol). The reaction mixture was stirred at room temperature for 12 h. The solvent was removed under reduced pressure, and the residue was thoroughly washed with diethyl ether. The residue was extracted with dichloromethane (5 mL), which was concentrated to ca. 2 mL. After careful addition of diethyl ether (ca. 2 mL), the solution was allowed to stand at 2 °C to afford orange crystals of $[Pt_3(\mu\text{-dpmp})_2(t\text{-BuNC})(XylNC)](PF_6)_2$ (**2**), which were separated by filtration, washed with diethyl ether, and dried in vacuo (52 mg, yield 52%). Anal. Calcd for $C_{78}H_{76}N_2P_8F_{12}Pt_3$: C, 44.56; H, 3.64; N, 1.33. Found: C, 44.66; H, 3.73; N, 1.32. IR (Nujol): 2170, 2142 (N≡C), 836 (PF_6) cm^{-1}. UV−vis (in CH_2Cl_2): λ_{max} (log ϵ) 497 (2.90), 388 (4.21), 359 (4.14), 297 (4.02) nm. ^1H NMR (in CD_2Cl_2): δ 0.38 (s, *t*-Bu, 9H), 1.41 (s, *o*-Me, 6H), 4.5−5.1 (m, CH_2, 8H), 6.8−8.0 (m, Ar, 53H). $^{31}P\{^1H\}$ NMR (in CD_2Cl_2): δ −16.6 (m, 2P, $^1J_{PtP}$ = 2819 Hz), −0.6 (m, 1P, $1J_{PtP}$ = 2949), 1.3 (m, 2P, $^1J_{PtP}$ = 2958 Hz), 2.8 (m, 1P, $1J_{PtP}$ = 3013).

Preparation of $[Pt_3(\mu\text{-dpmp})_2(t\text{-BuNC})_2](PF_6)_2$ (4). By a procedure similar to that for **3**, using **1** (54 mg, 0.024 mmol) and *t*-BuNC (2.0 mmol), orange single crystals of $[Pt_3(\mu\text{-dpmp})_2(t\text{-BuNC})_2](PF_6)_2$ (**4**) were isolated (40 mg, yield 81%). Anal. Calcd for $C_{74}H_{76}N_2P_8F_{12}Pt_3$: C, 43.26; H, 3.73; N, 1.36. Found: C, 43.44; H, 3.59; N, 1.35. IR (Nujol): 2163 (N≡C), 834 (PF_6) cm^{-1}. UV−vis (in CH_2Cl_2): λ_{max} (log ϵ) 496 (2.69), 386 (4.03), 357 (3.99), 310 (3.81), 297 (3.86) nm. ^1H NMR (in acetone-d_6): δ 0.51 (s, *t*-Bu, 18H), 4.8−5.3 (m, CH_2, 8H), 7.0−8.1 (m, Ar, 50H). $^{31}P\{^1H\}$ NMR (in CD_2Cl_2): δ −16.8 (m, 2P, $^1J_{PtP}$ = 2832 Hz), 0.7 (m, 4P, $1J_{PtP}$ = 3000).

Preparation of $[Pt_3(\mu\text{-dpmp})_2(TolNC)_2](PF_6)_2$ (5). All procedures were carried out in a glovebox filled with pure nitrogen. A benzene solution (0.21 M) of *p*-tolyl isocyanide

(3) (a) Irwin, M. J.; Jia, G.; Vittal, J.; Puddephatt, R. J. *Organometallics* **1996**, *15*, 5321. (b) Bradford, A. M.; Kristof, E.; Rashidi, M.; Yang, D. S.; Payne, N. C.; Puddephatt, R. J. *Inorg. Chem.* **1994**, *33*, 2355.

(4) For example: (a) Ren, T.; Zou, G.; Alvarez, J. C. *Chem. Commun.* **2000**, 1997. (b) Wong, K.-T.; Lehn, J.-M.; Peng, S.-M.; Lee, G.-H. *Chem. Commun*. **2000**, 2259. (c) Bruce, M. I.; Smith, M. E.; Zaitseva, N. N.; Skelton, B. W.; White, A. H. *J. Organomet. Chem*. **2003**, *670*, 170. (d) Leoni, P.; Marchetti, F.; Marchetti, L.; Pasquali, M. *Chem. Commun*. **2003**, 2372.

(5) (a) Tanase, T.; Begum, R. A.; Toda, H.; Yamamoto, Y. *Organometallic* **2001**, *20*, 968. (b) Tanase, T.; Begum, R. A. *Organometallics* **2001**, *20*, 106. (c) Tanase, T.; Hamaguchi, M.; Begum, R. A.; Goto, E. *Chem. Commun.* **2001**, 1072. (d) Tanase, T.; Hamaguchi, M.; Begum, R. A.; Yano, S.; Yamamoto, Y. *Chem. Commun.* **1999**, 745. (e) Tanase, T.; Ukaji, H.; Takahata, H.; Toda, T.; Yamamoto, Y. *Organometallics* **1998**, *17*, 196. (f) Tanase, T.; Toda, T.; Yamamoto, Y. *Inorg. Chem.* **1997**, *36*, 1571. (g) Tanase, T.; Takahata, H.; Ukaji, H.; Hasegawa, M.; Yamamoto, Y. *J. Organomet. Chem.* **1997**, *538*, 247. (h) Tanase, T.; Igoshi, T.; Yamamoto, Y. *Inorg. Chim. Acta* **1997**, *256*, 61. (i) Tanase, T.; Takahata, H.; Yamamoto, Y. *Inorg. Chim. Acta* **1997**, *264*, 5. (j) Tanase, T.; Takahata, H.; Hasegawa, M.; Yamamoto, Y. *J. Organomet. Chem.* **1997**, *545/546*, 531. (k) Tanase, T.; Ukaji, H.; Igoshi, T.; Yamamoto, Y. *Inorg. Chem.* **1996**, *35*, 4114.

(6) Ugi, I.; Fetzer, U.; Eholzer, U.; Knupfer, H.; Offerman, K. *Angew. Chem., Int. Ed. Engl.* **1965**, *4*, 472.

(TolNC) (0.042 mmol) was added to a dichloromethane solution containing **1** (31 mg, 0.014 mmol), which was stirred for 8 h. The color of the solution changed from orange to dark green, and the solvent was removed under reduced pressure. The residue was crystallized from an acetone/diethyl ether solution to afford green microcrystals of $[Pt_3(\mu\text{-dpmp})_2(TolNC)_2](PF_6)_2 \cdot (CH_3)_2CO$ (**5**·$(CH_3)_2CO$), which were separated by filtration, washed with diethyl ether, and dried in vacuo (26 mg, yield 85%). Anal. Calcd for $C_{83}H_{78}N_2OP_8F_{12}Pt_3$: C, 45.72; H, 3.61; N, 1.28. Found: C, 46.08; H, 3.49; N, 1.59. IR (Nujol): 2138 (N≡C), 838 (PF_6) cm^{-1}. UV−vis (in CH_2Cl_2): λ_{max} (log ϵ) 617 (2.77), 388 (4.08), 363 (4.05), 299 (4.03) nm. ^1H NMR (in CD_2Cl_2): δ 1.46 (s, *p*-Me, 6H), 4.5−5.1 (m, CH_2, 8H), 6.7−8.0 (m, Ar, 58H). $^{31}P\{^1H\}$ NMR (in CD_2Cl_2): δ −16.7 (m, 2P, $^1J_{PtP}$ = 2809 Hz), 0.7 (m, 4P, $1J_{PtP}$ = 2974).

Preparation of $[Pt_3(\mu\text{-dpmp})_2(XylNC)_2]I_2$ (6a). To a dichloromethane solution (10 mL) containing **1** (61 mg, 0.028 mmol) was added a methanolic solution (10 mL) of KI (59 mg, 0.36 mmol). The solution was stirred at room temperature for 12 h. The solvent was removed under reduced pressure, and the residue was washed with methanol. The residue was crystallized from a dichloromethane/diethyl ether mixed solvent to afford reddish orange crystals of $[Pt_3(\mu\text{-dpmp})_2(XylNC)_2]I_2$ (**6a**) (53 mg, yield 88%). Anal. Calcd for $C_{82}H_{76}N_2P_6Pt_3I_2$: C, 46.58; H, 3.62; N, 1.32. Found: C, 46.08; H, 3.94; N, 1.53. IR (Nujol): 2139, 2109 (N≡C) cm^{-1}. UV−vis (in CH_2Cl_2): λ_{max} (log ϵ) 500 (3.67), 391 (4.98), 360 (4.86), 297 (4.81) nm. ^1H NMR (in CD_2Cl_2): δ 1.40 (s, *o*-Me, 12H), 5.1−5.2 (m, CH_2, 8H), 6.7−8.2 (m, Ar, 56H). $^{31}P\{^1H\}$ NMR (in CD_2Cl_2): δ −15.7 (m, 2P, $^1J_{PtP}$ = 2785 Hz), 2.3 (m, 4P, $^1J_{PtP}$ = 2962 Hz). Recrystallization of **6a** from an acetone/diethyl ether mixed solvent yielded large block-shaped crystals of **6a**·$(CH_3)_2CO \cdot Et_2O$, which were suitable for X-ray crystallography.

Preparation of $[Pt_3(\mu\text{-dpmp})_2(XylNC)_2](BPh_4)_2$ (6b). By a procedure similar to that for **6a**, using **1** (43 mg, 0.020 mmol) and $NaBPh_4$ (138 mg, 0.40 mmol), orange microcrystals of $[Pt_3(\mu\text{-dpmp})_2(XylNC)_2](BPh_4)_2$ (**6b**) were obtained (34 mg, yield 67%). Anal. Calcd for $C_{130}H_{116}N_2P_6B_2Pt_3$: C, 62.48; H, 4.68; N, 1.12. Found: C, 62.38; H, 4.86; N, 1.13. IR (Nujol): 2132 (N≡C) cm^{-1}. UV−vis (in CH_2Cl_2): λ_{max} (log ϵ) 501 (3.63), 390 (5.00), 359 (4.91), 296 (4.93) nm. ^1H NMR (in acetone-d_6): δ 1.52 (s, *o*-Me, 12H), 5.0−5.2 (m, CH_2, 8H), 6.7−8.0 (m, Ar, 76H). $^{31}P\{^1H\}$ NMR (in CD_2Cl_2): δ −15.8 (m, 2P, $^1J_{PtP}$ = 2792 Hz), 2.0 (m, 4P, $^1J_{PtP}$ = 2972).

Preparation of $[Pt_3(\mu\text{-dpmp})_2(XylNC)_2][Pt(CN)_4]$ (6c). A methanolic solution (5 mL) of $K_2[Pt(CN)_4]$ (22 mg, 0.058 mmol) was added to a dichloromethane solution (20 mL) of **1** (120 mg, 0.054 mmol). The mixture was heated to reflux for 20 h. The solvent was removed under reduced pressure, and the residue was crystallized from CH_3CN/Et_2O to afford reddish orange crystals of $[Pt_3(\mu\text{-dpmp})_2(XylNC)_2][Pt(CN)_4]$ (**6c**), which were separated by filtration, washed with diethyl ether, and dried in vacuo (76 mg, yield 65% with respect to **1**). Anal. Calcd for $C_{86}H_{76}N_6P_6Pt_4$: C, 47.83; H, 3.55; N, 3.89. Found: C, 47.60; H, 3.67; N, 3.72. IR (Nujol): 2140 (XylN≡C), 2124 (C≡N) cm^{-1}. UV−vis (in CH_2Cl_2): λ_{max} (log ϵ) 497 (3.10), 388 (4.28), 359 (4.22) nm. ^1H NMR (in DMF-d_7): δ 1.53 (s, *o*-Me, 12H), 4.8−5.5 (m, CH_2, 8H), 6.8−8.2 (m, Ar, 56H). $^{31}P\{^1H\}$ NMR (in DMF-d_7): δ −15.4 (m, 2P, $^1J_{PtP}$ = 2776 Hz), 2.5 (m, 4P, $1J_{PtP}$ = 2973).

Preparation of $\{[Pt_3(\mu\text{-dpmp})_2(bisNC1)](PF_6)_2\}_n$ (7a). A dichloromethane solution (4 mL) of 2,3,5,6-tetramethylphenylene-1,4-bisisocyanide (bisNC1) (0.122 mmol) was slowly added to a dichloromethane solution (6 mL) of **1** (142 mg, 0.064 mmol). The solution was allowed to stand at room temperature for several hours to afford block-shaped orange crystals of $\{[Pt_3(\mu\text{-dpmp})_2(bisNC1)](PF_6)_2\}_n$ (**7a**), which were separated by filtration, washed with dichloromethane and diethyl ether, and dried under vacuum (106 mg, yield 80% with respect to **1**). Anal. Calcd for $C_{76}H_{70}N_2P_8F_{12}Pt_3$: C, 44.05; H, 3.40; N, 1.35. Found: C, 44.39; H, 3.64; N, 1.33. IR (Nujol): 2125 br (N≡C), 836 (PF_6) cm^{-1}. UV−vis (in CH_3CN): λ_{max} (log ϵ) 501 (2.68), 393 (3.95), 361 (3.96), 300 (4.06) nm. ^1H NMR (in CD_3CN): δ 1.09 (s, Me, 12H), 4.4−5.1 (m, CH_2, 8H), 6.7−7.9 (m, Ar, 50H). $^{31}P\{^1H\}$ NMR (in CD_3CN): δ −15.9 (m, 2P, $^1J_{PtP}$ = 2790 Hz), 1.7 (m, 4P, $^1J_{PtP}$ = 2972).

Preparation of $\{[Pt_3(\mu\text{-dpmp})_2(bisNC1)]I_2 \cdot CH_2Cl_2\}_n$ (7b). A dichloromethane solution (1 mL) of 2,3,5,6-tetramethylphenylene-1,4-bisisocyanide (bisNC1) (0.05 mmol) was slowly added to a dichloromethane solution (3 mL) of **6a** (26 mg, 0.012 mmol). The solution was allowed to stand at room temperature for several hours to afford block-shaped orange crystals of $\{[Pt_3(\mu\text{-dpmp})_2(bisNC1)]I_2 \cdot CH_2Cl_2\}_n$ (**7b**), which were separated by filtration, washed with dichloromethane and diethyl ether, and dried under vacuum (14 mg, yield 56%). Anal. Calcd for $C_{77}H_{72}N_2P_6Cl_2I_2Pt_3$: C, 43.60; H, 3.42; N, 1.32. Found: C, 43.41; H, 3.64; N, 1.49. IR (Nujol): 2112 br (N≡C) cm^{-1}. UV−vis (in CH_3CN): λ_{max} (log ϵ) 507 (3.44), 436 (4.28), 391 (4.71), 360 (4.83) nm. ^1H and ^{31}P NMR spectra were not measured owing to low solubility.

Preparation of $\{[Pt_3(\mu\text{-dpmp})_2(bisNC2)](PF_6)_2\}_n$ (7c). A dichloromethane solution (2 mL) of 3,3′,5,5′-tetramethylbiphenylene-4,4′-bisisocyanide (bisNC2) (0.046 mmol) was slowly added to a dichloromethane solution (5 mL) of **1** (107 mg, 0.048 mmol). The solution was allowed to stand at room temperature for several hours to afford an orange powder of $\{[Pt_3(\mu\text{-dpmp})_2(bisNC2)](PF_6)_2\}_n$ (**7c**), which was separated by filtration, washed with dichloromethane and diethyl ether, and dried under vacuum (82 mg, yield 80%). Anal. Calcd for $C_{82}H_{74}N_2P_8F_{12}Pt_3$: C, 45.84; H, 3.47; N, 1.30. Found: C, 45.98; H, 3.71; N, 1.28. IR (Nujol): 2132 (N≡C), 835 (PF_6) cm^{-1}. UV−vis (in CH_3CN): λ_{max} (log ϵ) 498 (2.90), 393 (4.20), 361 (4.79), 315 (4.28) nm. ^1H NMR (in CD_3CN): δ 1.46 (s, Me, 12H), 4.5−5.1 (m, CH_2, 8H), 6.7−8.0 (m, Ar, 54H). $^{31}P\{^1H\}$ NMR (in CD_3CN): δ −16.2 (m, 2P, $^1J_{PtP}$ = 2792 Hz), 1.5 (m, 4P, $^1J_{PtP}$ = 2980).

Preparation of $[(bisNCn)Pt_3(\mu\text{-dpmp})_2(bisNCn)Pt_3(\mu\text{-dpmp})_2(bisNCn)](PF_6)_4$ (n = 3 (8a), 4 (8b)). All procedures were carried out in a glovebox filled with pure nitrogen. A dichloromethane solution (4 mL) of phenylene-1,4-bisisocyanide (bisNC3) (0.037 mmol) was slowly added to a dichloromethane solution (6 mL) of **1** (44 mg, 0.020 mmol). The mixture was allowed to stand at room temperature for 3 h. The dark green powder of $[(bisNC3)Pt_3(\mu\text{-dpmp})_2(bisNC3)Pt_3(\mu\text{-dpmp})_2(bisNC3)](PF_6)_4$ (**8a**) was separated by filtration, washed with dichloromethane and diethyl ether, and dried under vacuum (40 mg, yield 96%). Anal. Calcd for $C_{152}H_{128}N_6P_{16}F_{24}Pt_6$: C, 43.88; H, 3.10; N, 2.02. Found: C, 44.03; H, 3.16; N, 2.25. IR (Nujol): 2136 (N≡C), 1622 br (N=C), 841 (PF_6) cm^{-1}. UV−vis (in CH_3CN): λ_{max} (log ϵ) 605 (2.94), 388 (3.67), 365 (3.70) nm. ^1H and ^{31}P NMR spectra were not measured owing to low solubility. Following the same procedure for **8a** but using 2,5-dimethylphenylene-1,4-bisisocyanide (bisNC4), a green powder of $[(bisNC4)Pt_3(\mu\text{-dpmp})_2(bisNC4)Pt_3(\mu\text{-dpmp})_2(bisNC4)](PF_6)_4$ (**8b**) was obtained (40 mg, yield 94%). Anal. Calcd for $C_{158}H_{140}N_6P_{16}F_{24}Pt_6$: C, 44.71; H, 3.32; N, 1.98. Found: C, 44.51; H, 3.48; N, 2.31. IR (Nujol): 2119 (N≡C), 1635 br (N=C), 840 (PF_6) cm^{-1}. UV−vis (in CH_3CN): λ_{max} (log ϵ) 610 (2.87), 390 (4.14), 363 (4.16) nm.

Preparation of $[Pt_3(\mu\text{-NO})_2(\mu\text{-dpmp})_2(RNC)_2](BF_4)_4$ (R = Xyl (10a), Mes (10b)). To a dichloromethane (20 mL) solution containing complex **1** (100 mg, 0.045 mmol) was added $[NO][BF_4]$ (27 mg, 0.23 mmol). The reaction solution was stirred at room temperature for 3 h while its color changed from orange to pale green. The solution was concentrated to ca. 3 mL and was allowed to stand at 2 °C to afford block-shaped pale green crystals of $[Pt_3(\mu\text{-NO})_2(\mu\text{-dpmp})_2(XylNC)_2](BF_4)_4 \cdot CH_2Cl_2$ (**10a**·CH_2Cl_2) in 66% yield (70 mg). Anal. Calcd for $C_{83}H_{78}O_2N_4P_6B_4F_{16}Cl_2Pt_3$: C, 42.37; H, 3.34; N, 2.38. Found: C, 42.29; H, 3.45; N, 2.01. IR (KBr): 2206 (N≡C), 1514 (NO), 1100 (BF_4) cm^{-1}. UV−vis (in CH_3CN): λ_{max} (log ϵ) 332 (3.69) nm. A similar procedure using complex **2** (43 mg)

afforded pale green crystals of $[Pt_3(\mu\text{-dpmp})_2(\mu\text{-NO})_2(MesNC)_2](BF_4)_4\cdot 2CH_2Cl_2$ (**10b**·$2CH_2Cl_2$) in 68% yield (33 mg). Anal. Calcd for $C_{86}H_{84}O_2N_4P_6B_4F_{16}Cl_4Pt_3$: C, 41.89; H, 3.43; N, 2.27. Found: C, 42.02; H, 3.45; N, 1.98. IR (KBr): 2205 (N≡C), 1513 (NO), 1083 (BF_4) cm^{-1}. UV−vis (in CH_3CN): λ_{max} (log ϵ) 330 (3.80) nm. ^1H and ^{31}P NMR spectra of compounds **10a** and **10b** were not measured owing to low solubility.

Preparation of $[Pt_3(\mu\text{-}C_{12}N_8)(\mu\text{-dpmp})_2(RNC)_2](PF_6)_2$ (R = Xyl (11a), Mes (11b)). To a dichloromethane (20 mL) solution of **1** (71 mg, 0.032 mmol) was added 37 mg (0.29 mmol) of tetracyanoethylene (tcne). The reaction solution was stirred at room temperature for 1 h while the color of the solution immediately changed from orange to pale green. The solvent was removed under reduced pressure, and the residue was washed with benzene and diethyl ether and was then extracted with 20 mL of dichloromethane. The solution was concentrated to ca. 2 mL and was kept at 2 °C after addition of a small amount of Et_2O to afford block-shaped pale green crystals of $[Pt_3(\mu\text{-dpmp})_2(\mu\text{-}C_{12}N_8)(XylNC)_2](PF_6)_2$ (**11a**) in 86% yield (67 mg). Anal. Calcd for $C_{94}H_{76}N_{10}P_8F_{12}Pt_3$: C, 46.91; H, 3.18; N, 5.82. Found: C, 46.67; H, 3.30; N, 5.54. IR (Nujol): 2189, 2168 (XylN≡C), 1571 (C=C), 840 (PF_6) cm^{-1}. UV−vis (in CH_2Cl_2): λ_{max} (log ϵ) 404 (3.22) nm. ^1H NMR (in CD_2Cl_2): δ 1.34, 1.98 (s, *o*-Me, 6H), 2.9−5.5 (m, CH_2, 8H), 6.1−8.8 (m, Ar, 56H). $^{31}P\{^1H\}$ NMR (in CD_2Cl_2): δ −5.7 (m, 2P, $^1J_{PtP}$ = 2450 Hz), 0.2 (m, 2P, $1J_{PtP}$ = 2906 Hz), 6.1 (m, 2P, $^1J_{PtP}$ = 2556 Hz). Recrystallization of **11a** from an acetone/diethyl ether mixed solvent yielded block-shaped crystals of **11a**·$(CH_3)_2CO$, which were suitable for X-ray crystallography. A similar procedure using complex **2** (62 mg) afforded pale green crystals of $[Pt_3(\mu\text{-dpmp})_2(\mu\text{-}C_{12}N_8)(MesNC)_2](PF_6)_2\cdot CH_2Cl_2$ (**11b**·CH_2Cl_2) in 38% yield (27 mg). Anal. Calcd for $C_{97}H_{82}N_{10}P_8F_{12}Cl_2Pt_3$: C, 46.24; H, 3.28; N, 5.56. Found: C, 46.48; H, 3.08; N, 5.70. IR (Nujol): 2186, 2169 (MesN≡C), 1573 (C=C), 838 (PF_6) cm^{-1}. UV−vis (in CH_2Cl_2): λ_{max} (log ϵ) 391 (3.37) nm. ^1H NMR (in CD_2Cl_2): δ 1.28, 1.90 (s, *o*-Me, 6H), 2.06, 2.20 (s, *p*-Me, 3H), 3.4−5.2 (m, CH_2, 8H), 6.2−8.6 (m, Ar, 54H). $^{31}P\{^1H\}$ NMR (in CD_2Cl_2): δ −7.3 (m, 2P, $^1J_{PtP}$ = 2514 Hz), −1.6 (m, 2P, $1J_{PtP}$ = 2926 Hz), 4.2 (m, 2P, $^1J_{PtP}$ = 2571 Hz).

Preparation of $\{[Pt_3(\mu\text{-H})(\mu\text{-dpmp})_2(bisNC1)](BF_4)_3\}_n$ (13), $\{[Pt_3(\mu\text{-NO})_2(\mu\text{-dpmp})_2(bisNC1)](BF_4)_4\}_n$ (14), $\{[Pt_3(\mu\text{-}C_{12}N_8)(\mu\text{-dpmp})_2(bisNC1)](PF_6)_2\}_n$ (15), and $\{[Pt_3(\mu\text{-}R^1C_2R^2)(\mu\text{-dpmp})_2(bisNC1)](PF_6)_2\}_n$ (16a, R^1 = H, R^2 = $COOCH_3$; 16b, R^1 = R^2 = $COOCH_3$). To a suspension of compound **7a** (50 mg) in acetonitrile or/and dichloromethane was added an excess of HBF_4, $NOBF_4$, tcne, or $R^1C{\equiv}CR^2$ (R^1 = H, $COOCH_3$; R^2 = $COOCH_3$), and the mixture was stirred at room temperature for 1−3 h. The resultant pale yellow-green to brown powder was collected, washed with CH_2Cl_2 and Et_2O, and dried under vacuum. For **13**·CH_2Cl_2: yield 64% (33 mg). Anal. Calcd for $C_{77}H_{73}N_2P_6B_3F_{12}Cl_2Pt_3$: C, 43.44; H, 3.46; N, 1.32. Found: C, 43.23; H, 3.38; N, 1.25. IR (Nujol): 2197 sh, 2161 br (N≡C), 1084 (BF_4) cm^{-1}. UV−vis (in CH_3CN): λ_{max} (log ϵ) 323 (4.01) nm. For **14**·$3CH_2Cl_2$: yield 57% (34 mg). Anal. Calcd for $C_{79}H_{76}N_4O_2P_6B_4F_{16}Cl_6Pt_3$: C, 38.82; H, 3.13; N, 2.29. Found: C, 38.55; H, 3.36; N, 2.57. IR (KBr): 2196 br (N≡C), 1484 (NO), 1084 (BF_4) cm^{-1}. UV−vis (in CH_3CN): λ_{max} (log ϵ) 356 (3.69) nm. For **15**·$2CH_3CN\cdot CH_2Cl_2$: yield 70% (42 mg). Anal. Calcd for $C_{93}H_{78}N_{12}P_8F_{12}Cl_2Pt_3$: C, 44.76; H, 3.15; N, 6.73. Found: C, 44.59; H, 3.19; N, 6.76. IR (Nujol): 2181 br, 2161 br (N≡C), 1585 (C=C), 840 (PF_6) cm^{-1}. UV−vis (in CH_3CN): λ_{max} (log ϵ) 400 (3.22) nm. For **16a**: yield 58% (30 mg). Anal. Calcd for $C_{80}H_{74}N_2O_2P_8F_{12}Pt_3$: C, 44.56; H, 3.46; N, 1.30. Found: C, 44.56; H, 3.51; N, 1.36. IR (Nujol): 2161 sh, 2110 br (N≡C), 1674 br (C=O, C=C), 838 (PF_6) cm^{-1}. UV−vis (in CH_3CN): λ_{max} (log ϵ) 398 (3.59), 358 (3.80) nm. For **16b**: yield 74% (40 mg). Anal. Calcd for $C_{82}H_{76}N_2O_4P_8F_{12}Pt_3$: C, 44.47; H, 3.46; N, 1.26. Found: C, 44.66; H, 3.66; N, 1.19. IR (Nujol): 2157 sh, 2121 br (N≡C), 1719, 1688 br (C=O, C=C), 837 (PF_6) cm^{-1}. UV−vis (in CH_3CN): λ_{max} (log ϵ) 355 (3.91) nm. ^1H and ^{31}P NMR spectra of compounds **13**−**16** were not measured owing to low solubility.

Table 1. Crystallographic and Experimental Data for 2·2{$(CH_3)_2CO$} and 3·2.5CH_2Cl_2

	2·2{$(CH_3)_2CO$}	**3**·2.5CH_2Cl_2
formula	$C_{90}H_{92}N_2P_8F_{12}O_2Pt_3$	$C_{80.5}H_{81}N_2P_8F_{12}Cl_5Pt_3$
fw	2294.77	2314.84
diffractometer	AFC7R	AFC7R
cryst syst	monoclinic	monoclinic
space group	$P2_1/a$ (No. 14)	$P2_1$ (No. 4)
a, Å	14.133(4)	15.167(4)
b, Å	22.108(6)	13.976(3)
c, Å	29.505(8)	21.634(3)
α, deg		
β, deg	90.70(3)	108.01(1)
γ, deg		
V, Å^3	9087(4)	4361(1)
Z	4	2
T, °C	−118	−118
D_{calcd}, g cm^{-3}	1.677	1.763
abs coeff, cm^{-1}	48.01	51.49
2θ range, deg	$4 < 2\theta < 45$	$4 < 2\theta < 50$
no. of unique data	11 775	7936
no. of obsd data	7748 ($I > 2\sigma(I)$)	5363 ($I > 2\sigma(I)$)
no. of variables	1055	540
R^a	0.051	0.058
R_w or $wR2$	0.054[b]	0.064[b]

[a] $R = \sum||F_o| - |F_c||/\sum|F_o|$. [b] $R_w = [\sum w(|F_o| - |F_c|)^2/\sum w|F_o|^2]^{1/2}$ ($w = 1/\sigma^2(F_o)$).

Table 2. Crystallographic and Experimental Data for 4 and 6a·$Et_2O\cdot(CH_3)_2CO$

	4	**6a**·$Et_2O\cdot(CH_3)_2CO$
formula	$C_{74}H_{76}N_2P_8F_{12}Pt_3$	$C_{89}H_{92}N_2P_6I_2O_2Pt_3$
fw	2054.47	2246.64
diffractometer	AFC7R	AFC7R
cryst syst	triclinic	monoclinic
space group	$P\bar{1}$ (No. 2)	$P2_1/n$ (No. 14)
a, Å	13.543(6)	16.420(3)
b, Å	13.921(5)	14.653(4)
c, Å	11.255(4)	38.26(1)
α, deg	100.33(3)	
β, deg	110.71(4)	96.96(2)
γ, deg	101.94(3)	
V, Å^3	1866(1)	9137(3)
Z	1	4
T, °C	−118	−118
D_{calcd}, g cm^{-3}	1.828	1.633
abs coeff, cm^{-1}	58.30	53.89
2θ range, deg	$4 < 2\theta < 50$	$4 < 2\theta < 45$
no. of unique data	6573	11 224
no. of obsd data	4280 ($I > 3\sigma(I)$)	7070 ($I > 2\sigma(I)$)
no. of variables	449	473
R^a	0.040	0.062
R_w or $wR2$	0.044[b]	0.078[b]

[a] $R = \sum||F_o| - |F_c||/\sum|F_o|$. [b] $R_w = [\sum w(|F_o| - |F_c|)^2/\sum w|F_o|^2]^{1/2}$ ($w = 1/\sigma^2(F_o)$).

X-ray Crystallography for 2·2{$(CH_3)_2CO$}, 3·2.5CH_2Cl_2, 4, 6a·$Et_2O\cdot(CH_3)_2CO$, 6c·$2CH_3CN$, 7a·$3CH_2Cl_2$. 9b·$5CH_2Cl_2$, 10a·$CH_2Cl_2\cdot 3H_2O$, and 11a·$(CH_3)_2CO$. All the crystals were extremely delicate when separated from their mother liquors, and the crystals used in data collection were mounted on top of a glass fiber with Paraton N oil at low temperature. The crystal of **7a**·$3CH_2Cl_2$ was sealed into a capillary along with a small amount of mother liquor and fixed at low temperature. Crystal data and experimental conditions are summarized in Tables 1−5. All data were collected on a Rigaku AFC7R diffractometer (for **2**, **3**, **4**, **6c**, **10a**, and **11a**) and a Rigaku AFC8R/Mercury CCD diffractometer (for **7a** and **9b**) equipped with graphite-monochromated Mo Kα (λ = 0.71069 Å) radiation at low temperature. The CCD image data were processed

Table 3. Crystallographic and Experimental Data for 6c·2CH_3CN and 7a·3CH_2Cl_2

	6c·2CH_3CN	**7a**·3CH_2Cl_2
formula	$C_{90}H_{82}N_8P_6Pt_4$	$C_{79}H_{76}N_2P_8F_{12}Cl_6Pt_3$
fw	2241.89	2327.24
diffractometer	AFC7R	AFC8R/Mercury CCD
cryst syst	orthorhombic	monoclinic
space group	$Pna2_1$ (No. 33)	$P2_1/c$ (No. 14)
a, Å	25.529(5)	23.511(3)
b, Å	15.742(3)	17.137(2)
c, Å	21.491(4)	25.919(4)
α, deg		
β, deg		111.174(6)
γ, deg		
V, Å^3	8636(2)	9738(2)
Z	4	4
T, °C	−118	−120
D_{calcd}, g cm^{-3}	1.724	1.587
abs coeff, cm^{-1}	65.92	46.39
2θ range, deg	$4 < 2\theta < 50$	$6 < 2\theta < 52$
no. of unique data	7490	19 101
no. of obsd data	6532 ($I > 2\sigma(I)$)	8590 ($I > 2\sigma(I)$)
no. of variables	975	619
R^a	0.031	0.084
R_w or $wR2$	0.035[b]	0.091[b]

[a] $R = \sum||F_o| - |F_c||/\sum|F_o|$. [b] $R_w = [\sum w(|F_o| - |F_c|)^2/\sum w|F_o|^2]^{1/2}$ ($w = 1/\sigma^2(F_o)$).

Table 4. Crystallographic and Experimental Data for 9b·5CH_2Cl_2 and 10a·CH_2Cl_2·3H_2O

	9b·5CH_2Cl_2	**10a**·CH_2Cl_2·3H_2O
formula	$C_{87}H_{87}N_2P_9F_{18}Cl_{10}Pt_3$	$C_{83}H_{84}N_4O_5P_6B_4F_{16}Cl_2Pt_3$
fw	2721.19	2406.83
diffractometer	AFC8R/Mercury CCD	AFC7R
cryst syst	triclinic	monoclinic
space group	$P\bar{1}$ (No. 2)	$P2_1/c$ (No. 14)
a, Å	14.472(2)	12.873(4)
b, Å	19.286(2)	29.350(6)
c, Å	19.696(2)	14.826(4)
α, deg	95.347(3)	
β, deg	95.716(4)	110.49(3)
γ, deg	100.407(6)	
V, Å^3	5345.1(9)	5246(2)
Z	2	2
T, °C	−120	−116
D_{calcd}, g cm^{-3}	1.691	1.523
abs coeff, cm^{-1}	43.58	41.89
2θ range, deg	$6 < 2\theta < 55$	$4 < 2\theta < 50$
no. of unique data	23 648	9211
no. of obsd data	16146 ($I > 2\sigma(I)$)	6842 ($I > 3\sigma(I)$)
no. of variables	718	492
R^a	0.074	0.058
R_w or $wR2$	0.090[b]	0.072[b]

[a] $R = \sum||F_o| - |F_c||/\sum|F_o|$. [b] $R_w = [\sum w(|F_o| - |F_c|)^2/\sum w|F_o|^2]^{1/2}$ ($w = 1/\sigma^2(F_o)$).

using the Crystal Clear 1.3.5 program (Rigaku/MSC)[7] and corrected for Lorentz−polarization and absorption effects.

The structures of **2**, **3**, **4**, **6a**, **6c**, and **10a** were solved by direct methods (SIR92)[8] and refined on F using full-matrix least-squares techniques with teXsan.[9] The coordinates of all hydrogen atoms except those of lattice solvents were calculated at ideal positions with a C−H distance of 0.95 Å and were not refined. For **2**, **4**, and **6c**, final refinements were carried out with anisotropic thermal parameters for all non-hydrogen atoms. The structure refinement of **3** was carried out with anisotropic thermal parameters for the Pt, Cl, and P atoms and with isotropic parameters for other non-hydrogen atoms. The lattice CH_2Cl_2 molecules were disordered. For **6a**, the Pt, I, and P atoms were refined with anisotropic thermal parameters, and other non-hydrogen atoms were refined isotropically. In the refinement of **10a**, the BF_4 anions were treated as rigid groups due to large thermal motions, and other non-hydrogen atoms were refined anisotropically. The structure of **7a** was solved by heavy atom methods with DIRDIF94 PATTY.[10] The dpmp ligands were severely disordered and refined by a two-site model with each having 0.5 occupancy. The phenyl groups of dpmp were refined as rigid groups. This feature led to a low-grade refinement of the present X-ray analysis. Final refinement was carried out on F with anisotropic thermal parameters for the Pt, Cl, P, and F atoms and with isotropic ones for other non-hydrogen atoms (except for the rigid group atoms). The structure of **9b** was solved with DIRDIF94 PATTY and refined on F with teXsan; the Pt, Cl, P, and F atoms were refined with anisotropic thermal parameters and other non-hydrogen atoms with isotropic ones. The structure of **11a** was solved by DIRDIF94 PATTY and refined with SHELXL-93.[11] The non-hydrogen atoms of the phenyl rings and solvated acetone molecules were refined isotropically, and other non-hydrogen atoms were refined with anisotropic temperature factors. All calculations were carried out on a Silicon Graphics O2 station with the teXsan program system.[9]

Table 5. Crystallographic and Experimental Data for 11a·$(CH_3)_2CO$

formula	$C_{97}H_{82}N_{10}P_8F_{12}OPt_3$
fw	2464.82
diffractometer	AFC7R
cryst syst	monoclinic
space group	$P2_1/c$ (No. 14)
a, Å	13.872(4)
b, Å	53.16(1)
c, Å	15.130(4)
α, deg	
β, deg	97.90(2)
γ, deg	
V, Å^3	11 050(4)
Z	4
T, °C	−118
D_{calcd}, g cm^{-3}	1.481
abs coeff, cm^{-1}	39.55
2θ range, deg	$4 < 2\theta < 45$
no. of unique data	14 381
no. of obsd data	10 081 ($I > 2\sigma(I)$)
no. of variables	877
R^a	0.068
R_w or $wR2$	0.227[b]

[a] $R = \sum||F_o| - |F_c||/\sum|F_o|$. [b] $wR2 = [\sum w(F_o^2 - F_c^2)^2/\sum w(F_o)^2]^{1/2}$ (for all data, $w = 1/[\sigma^2(F_o) + (0.0889P)^2 + 230.9415P]$, $P = (F_o^2 + 2F_c^2)/3$).

EXAFS Analysis. X-ray absorption measurements around the Pt L_3 edge (10.856−13.056 keV with 586 steps) were carried out at the Photon Factory of the National Laboratory for High Energy Physics on beam line 10B using synchrotron radiation (2.5 GeV, 350−300 mA).[12] The experiments were done in the transmission mode on BN pellets of the powdered samples of complexes **1**, **2**, **4**, **5**, **7a**, **7c**, **8a**, and **8b** using a Si(311) monochromator. The theoretical expression of the obtained $\boldsymbol{k}^3\chi(\boldsymbol{k})$ for the case of single scattering is shown in eq 1 (see Supporting Information),[13] where $\boldsymbol{r}_i$, N_i, S_i, $F_i(\boldsymbol{k})$,

(7) *Crystal Clear 1.3.5*: Operating software for the CCD detector system; Rigaku and Molecular Structure Corp., 2003.

(8) Altomare, A.; Burla, M. C.; Camalli, M.; Cascarano, M.; Giacovazzo, C.; Guagliardi, A.; Polidori, G. *J. Appl. Crystallogr.* **1994**, *27*, 435.

(9) *TEXSAN*: Crystal Structure Analysis Package; Molecular Structure Corp., 1999.

(10) Beurskens, P. T.; Admiraal, G.; Beurskens, G.; Bosman, W. P.; de Gelder, R.; Israel, R.; Smits, J. M. M. *DIRDIFF-94* program system, Technical Report of the Crystallography Laboratory; University of Nijmegen: The Netherlands, 1994.

(11) Sheldrick, G. M. *SHELXL-93/97*, Program for the Refinement of Crystal Structures; University of Göettingen: Göettingen, Germany, 1996.

(12) *Photon Factory Activity Report*; National Laboratory for High Energy Physics: Ibaraki, Japan, 1986.

Scheme 1

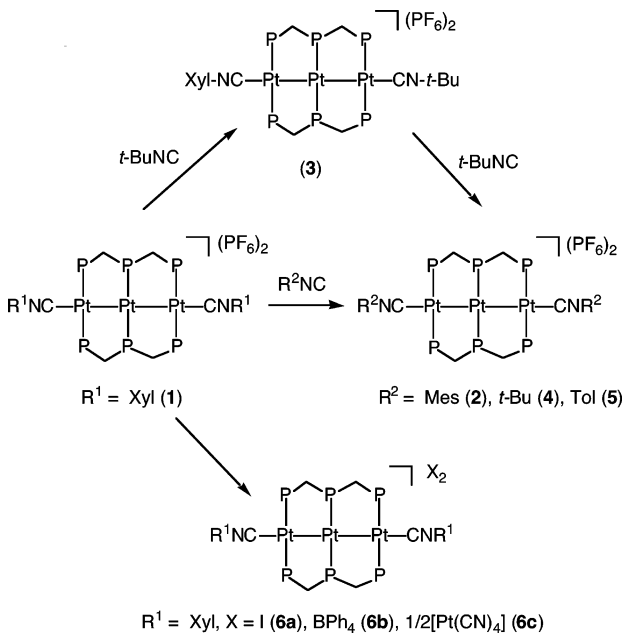

$\Phi_i(\boldsymbol{k})$, and σ_i represent the interatomic distance, the coordination number, the reducing factor, the backscattering amplitude, the phase shift, and the Debye−Waller factor, respectively, and $\boldsymbol{k}$ is the photoelectron wave vector defined as $\boldsymbol{k} = [(8\pi^2 m/h^2)(E - E_0)]^{1/2}$ (E_0 = 11.558 keV). The backscattering amplitude $F_i(\boldsymbol{k})$ and the phase shift $\Phi_i(\boldsymbol{k})$ functions used were the theoretical parameters tabulated by McKale et al.[14] Curve-fitting analyses with the three-wave model, $\boldsymbol{k}^3\chi_c(\boldsymbol{k}) = \boldsymbol{k}^3\chi_C(\boldsymbol{k}) + \boldsymbol{k}^3\chi_P(\boldsymbol{k}) + \boldsymbol{k}^3\chi_{Pt}(\boldsymbol{k})$, were carried out by varying N_i, $\boldsymbol{r}_i$,σ_i, and E_0 with the nonlinear least-squares techniques; the reducing factors S_i are determined by the analysis of **1**. All calculations were performed on a Hewlett-Packard work station model 712/60 with the EXAFS analysis program package, REX2 (Rigaku Co. Ltd.).[15]

Molecular Orbital Calculations. Single-point density functional calculations on the structures of the complex cations of **1**−**4** (determined by X-ray crystallography) were performed using the BECK3LYP method with the LANL2DZ basis set. All calculations were carried out on a Silicon Graphics Octane Station with the Gaussian 98 program package. Extended Hückel molecular orbital calculations were carried out by using the parameters of the Coulomb integrals and the orbital exponents taken from ref 16 on a Pentium PC computer. For the Pt d functions, double-ξ expansions were used. The fragment analyses were performed by using the program CACAO.[17]

Results and Discussion

Axial Ligand Exchange Reactions of $[Pt_3(\mu\text{-dpmp})_2(XylNC)_2](PF_6)_2$ (1) with Monoisocyanides. Axial xylyl isocyanide ligands of complex **1** were readily replaced by other isocyanide molecules to afford a series of linear triplatinum complexes (Scheme 1), whereas the XylNC ligands could not be substituted by any other type of ligands, such as phosphines, CO, acetylides, and halides. Reaction of complex **1** with a large excess of 2,4,6-mesityl or *tert*-butyl isocyanide at room temperature gave $[Pt_3(\mu\text{-dpmp})_2(RNC)_2](PF_6)_2$ (R = Mes (**2**), *t*-Bu (**4**)) in good yields. When complex **1** was reacted with a regulated amount of *t*-BuNC (<10 equiv), the asymmetric linear complex $[Pt_3(\mu\text{-dpmp})_2(XylNC)(t\text{-BuNC})](PF_6)_2$ (**3**) was obtained in 52% yield and was further converted into complex **4** with a large excess of *t*-BuNC. When complex **1** was reacted with less bulky 4-tolyl isocyanide (TolNC), the green-colored complex $[Pt_3(\mu\text{-dpmp})_2(TolNC)_2](PF_6)_2$ (**5**) was obtained, and it was notably unstable in comparison with complexes **1**−**4**.

Table 6. Structural Parameters for $[Pt_3(\mu\text{-dpmp})_2(R^1NC)(R^2NC)]X_2$ Determined by X-ray Crystallographic Analyses

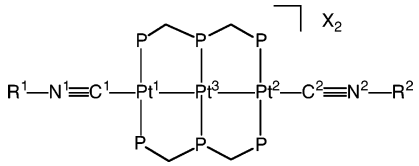

	1[a]	**2**	**3**
R^1	Xyl	Mes	Xyl
R^2	Xyl	Mes	*t*-Bu
X	PF_6	PF_6	PF_6
Pt^1-Pt^3, Å	2.724(2)	2.7134(9)	2.728(2)
Pt^2-Pt^3, Å	2.723(2)	2.7045(8)	2.696(2)
av Pt−Pt, Å	2.724	2.709	2.712
Pt^1-C^1, Å	1.93(2)	1.97(2)	1.85(3)
Pt^2-C^2, Å	1.99(3)	1.97(2)	1.94(3)
C^1-N^1, Å	1.25(3)	1.17(2)	1.29(3)
C^2-N^2, Å	1.21(3)	1.16(2)	1.22(4)
$Pt^1-Pt^3-Pt^2$, deg	178.66(8)	178.92(3)	176.39(6)
$Pt^1-C^1-N^1$, deg	169(2)	176(1)	165(2)
$Pt^2-C^2-N^2$, deg	168(2)	177(1)	172(3)
C^1-N^1-C, deg	174(3)	173(2)	169(3)
C^2-N^2-C, deg	175(3)	175(2)	176(4)

	4[b]	**6a**	**6c**
R^1	*t*-Bu	Xyl	Xyl
R^2	*t*-Bu	Xyl	Xyl
X	PF_6	I	1/2[$Pt(CN)_4$]
Pt^1-Pt^3, Å	2.696(1)	2.748(1)	2.7506(7)
Pt^2-Pt^3, Å	2.696(1)	2.717(1)	2.7696(7)
av Pt−Pt, Å	2.696	2.733	2.760
Pt^1-C^1, Å	1.98(1)	1.97(2)	2.00(1)
Pt^2-C^2, Å	1.98(1)	1.98(2)	2.01(1)
C^1-N^1, Å	1.14(1)	1.17(2)	1.18(2)
C^2-N^2, Å	1.14(1)	1.18(2)	1.18(2)
$Pt^1-Pt^3-Pt^2$, deg	180.0	177.19(4)	175.99(2)
$Pt^1-C^1-N^1$, deg	170(1)	176(2)	174(1)
$Pt^2-C^2-N^2$, deg	170(1)	175(2)	175(1)
C^1-N^1-C, deg	173(1)	175(2)	177(1)
C^2-N^2-C, deg	173(1)	179(2)	178(1)

[a] Ref 5e. [b] The structure has centro symmetry.

(i) Structures. The detailed structures of complexes **2**−**4** were determined by X-ray crystallography (ORTEP plots for the complex cations of **2** and **4** are deposited as Supporting Information, Figures S1 and S2), and the structural parameters of **1**−**4** are summarized in Table 6. The structure of complex **2** is quite similar to that of **1** with three platinum atoms linearly connected by metal−metal covalent bonds (Pt−Pt−Pt = 178.92(3)°) and symmetrically bridged by two dpmp ligands. The terminal sites of the Pt_3 core are ligated by two MesNC ligands. The Pt−Pt bond lengths are 2.7134(9) and 2.7045(9) Å (av 2.709 Å), which are appreciably shorter

(13) Sayers, D. E.; Stern, E. A.; Lytle, F. W. *Phys. Rev. Lett.* **1971**, *27*, 1204.
(14) McKale, A. G.; Veal, B. W.; Paulikas, A. P.; Chan, S. K.; Knapp, G. S. *J. Am. Chem. Soc.* **1988**, *110*, 3763.
(15) (a) Kosugi, N.; Kuroda, H. *REX*; Research Center for Spectrochemistry, the University of Tokyo: Tokyo, Japan, 1985. (b) *REX2*; Rigaku Co. Ltd.: Tokyo, Japan, 1995.
(16) (a) Hoffmann, R. *J. Chem. Phys.* **1963**, *39*, 1397. (b) Hoffmann, R.; Lipscomb, W. N. *J. Chem. Phys.* **1962**, *36*, 2179. (c) Hoffmann, R.; Lipscomb, W. N. *J. Chem. Phys.* **1962**, *36*, 3489. (d) Ammeter, J. H.; Burgi, H.-B.; Thibeault, J. C.; Hoffmann, R. *J. Am. Chem. Soc.* **1978**, *100*, 3686.
(17) Mealli, C.; Prosterpio, D. *J. Chem. Educ.* **1990**, 67, 399.

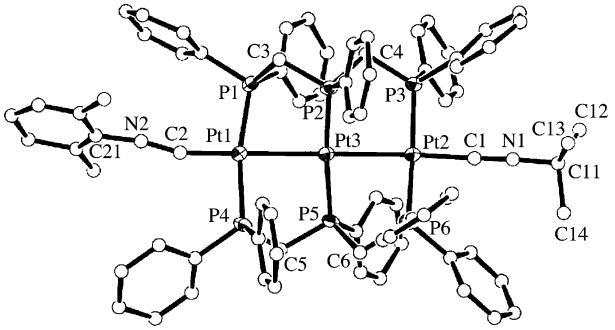

Figure 1. ORTEP plot of the complex cation of **3**, $[Pt_3(\mu\text{-dpmp})_2(XylNC)(t\text{-BuNC})](PF_6)_2$. The N and C atoms are drawn with arbitrary circles for clarity.

than those for complex **1** (av 2.724 Å),[5e] and the N≡C bond lengths (1.16(2) and 1.17(2) Å) are shorter than those in **1** (1.21(3) and 1.25(3) Å), suggesting that the extent of back-donation from the metal centers to the isocyanides became smaller in complex **2** compared with that of **1**. The structure of complex **4** involves a crystallographically imposed inversion center at the central Pt atom and possesses a linear triplatinum structure as found in **1** and **2**. The Pt−Pt bond length of 2.696(1) Å is significantly shorter than those found in **1** and **2**, and the N≡C bond length of 1.14(1) Å also indicates that the extent of back-donation from the Pt atoms is small. An important feature is demonstrated in the crystal structure of the asymmetric complex **3** (Figure 1). The Pt1−Pt3−Pt2 angle of 176.39(6)° indicated that the Pt_3 backbone is slightly bent in comparison with complexes **1**, **2**, and **4**. The Pt−Pt bond lengths are 2.728(2) Å (Pt1−Pt3) and 2.696(2) Å (Pt2−Pt3); the former value is comparable to those of **1**, and in contrast, the latter one is considerably shorter than those found in **1** but is equal to that of **4**. The N≡C bond length of XylNC (1.29(3) Å) is longer than that of *t*-BuNC (1.22(4) Å), while the Pt−C bond length of XylNC (1.85(3) Å) is shorter than the corresponding bond distance with *t*-BuNC (1.94(3) Å). Further, the coordination mode of XylNC (Pt1−C2−N2 = 165(2)°, C2−N2−C21 = 169(3)°) is quite bent compared to the *t*-BuNC ligand (Pt2−C1−N1 = 172(3)°, C1−N1−C11 = 176(4)°). These structural features clearly demonstrated the presence of a π *trans* influence of the terminal isocyanides. That is, with an increase in the π-acidity of the isocyanide ligand, the metal−metal bonding electrons may partially migrate into the π^* orbital of the CN unit, and consequently, the Pt−Pt bond length *trans* to the isocyanide increases.

Since single crystals of complex **5** were not obtained, the metal−metal bonded structural parameters were determined by extended X-ray absorption fine structure (EXAFS) analyses. The X-ray absorption spectra around the Pt L_3 edge were measured on the powdered samples of complexes **1**, **2**, **4**, and **5**. The Fourier transforms for all complexes showed identical patterns with three distinct peaks at about 1.5, 1.9, and 2.6 Å (before phase correction), which were assigned to the backscattering contributions of Pt−C, Pt−P, and Pt−Pt combinations on the basis of curve-fitting analyses (Figure S3 and Table 7). The structural parameters for **1**, **2**, and **4** were in agreement with the values determined by X-ray crystallography within an estimated error of 0.04 Å. In the case of complex **5**, the Pt−Pt separation was determined as 2.84(4) Å, which is longer by ca. 0.1 Å than those of complexes **1**, **2**, and **4** (2.72−2.73(4) Å). These results suggested that the less bulky aromatic isocyanide, *p*-TolNC, can interact strongly with the terminal Pt atom, and consequently, the increased extent of back-donation from the metal center to the C≡N π^* orbital resulted in a significantly elongated Pt−Pt bond distance.

Table 7. Structural Parameters Derived from EXAFS Analyses

complex	A−B[a]	N[b]	r, Å[c]	σ, Å[d]	R, %[e]
1	Pt−C	0.67[b]	1.92(3)	0.094	4.99
	Pt−P	2[b]	2.29(3)	0.044	
	Pt−Pt	1.33[b]	2.73(4)	0.065	
2	Pt−C	0.7	2.01(3)	0.069	4.18
	Pt−P	2.0	2.28(3)	0.040	
	Pt−Pt	1.4	2.72(4)	0.062	
4	Pt−C	0.6	1.90(3)	0.018	4.00
	Pt−P	2.4	2.28(3)	0.056	
	Pt−Pt	0.9	2.73(4)	0.058	
5	Pt−C	0.5	1.98(3)	0.031	3.39
	Pt−P	2.5	2.30(3)	0.063	
	Pt−Pt	1.2	2.84(4)	0.067	
7a	Pt−C	0.3	1.94(3)	0.043	3.88
	Pt−P	2.2	2.28(3)	0.050	
	Pt−Pt	1.5	2.71(4)	0.067	
7c	Pt−C	0.5	1.96(3)	0.064	4.33
	Pt−P	2.1	2.28(3)	0.045	
	Pt−Pt	1.3	2.72(4)	0.063	
8a	Pt−C	1.1	1.97(3)	0.104	4.82
	Pt−P	1.5	2.30(3)	0.036	
	Pt−Pt	1.4	2.85(4)	0.072	
8b	Pt−C	0.6	1.99(3)	0.041	2.95
	Pt−P	2.4	2.29(3)	0.032	
	Pt−Pt	1.4	2.86(4)	0.073	

[a] Assignable contributions; A is absorbing and B is backscattering atoms. [b] Coordination number referenced to complex **1**. Estimated errors are ±1. [c] Interatomic distances. Estimated errors are ±0.03 Å for the first and second shells (C, P) and ±0.04 Å for the third shell (Pt). [d] Debye−Waller factor. [e] $R = [\Sigma(\boldsymbol{k}^3\chi_o(\boldsymbol{k}) - \boldsymbol{k}^3\chi_c(\boldsymbol{k}))^2/\Sigma(\boldsymbol{k}^3\chi_o(\boldsymbol{k}))^2]^{1/2}$. $\chi_o(\boldsymbol{k})$ and $\chi_c(\boldsymbol{k})$ are Fourier-filtered observed and calculated data, respectively. $\boldsymbol{k}^3\chi_c(\boldsymbol{k}) = \boldsymbol{k}^3(\chi_C(\boldsymbol{k}) + \chi_P(\boldsymbol{k}) + \chi_{Pt}(\boldsymbol{k}))$.

(ii) Spectroscopy. The spectroscopic features of complexes **2**−**5** were consistent with the linear L−Pt−Pt−Pt−L structure as observed in complex **1**. The $^{31}P\{^1H\}$ NMR spectra of the symmetrical complexes **2**, **4**, and **5** exhibited two resonances with ^{195}Pt satellite peaks at δ 0.7−2.0 ($^1J_{PtP}$ = 2974−3000 Hz) for the outer P atoms of dpmp and δ −16.8 to −15.9 ($^1J_{PtP}$ = 2793−2832 Hz) for the central P atoms. The $^{31}P\{^1H\}$ NMR spectrum for complex **3** exhibited an asymmetrical A_2B_2-CC′ spectral pattern in an integration ratio of 2:2:1:1. In the electronic absorption spectra, all the complexes (**1**−**5**) showed a similar absorption pattern for the linear Pt_3 structure around 390−360 nm (Figure S4). The most characteristic absorption around 386−389 nm, assignable to $\sigma\rightarrow\sigma^*$ transition of the linear Pt_3 core, remained almost unvaried when the terminal isocyanide ligands were changed. For complexes **1**−**4**, a weak absorption was observed as the lowest energy transition at 496−499 nm, which may be assignable to a $\sigma\rightarrow\pi$ (HOMO−LUMO) transition in light of the MO calculations as described below. In complex **5**, the corresponding weak absorption significantly shifted to lower energy at 617 nm, suggesting that the HOMO−LUMO energy gap became appreciably smaller with the stronger π-accepting ability of *p*-TolNC ligands.

Single-point MO calculations using the DFT method were performed on the crystal structures of the complex

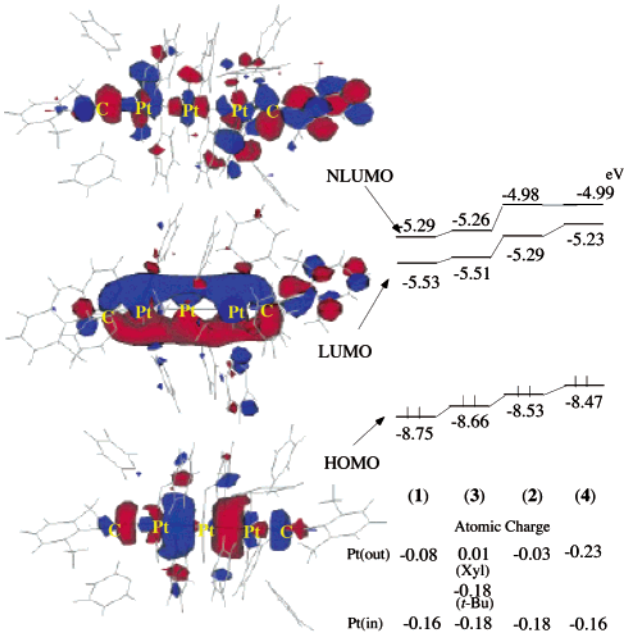

Figure 2. Perspective views of DFT calculated HOMO, LUMO, and next LUMO (NLUMO) for the cation of $[Pt_3(\mu\text{-dpmp})_2(XylNC)_2]^{2+}$ (**1**), along with diagrams showing the relative energy levels (eV) of the MOs and atomic charges of the outer and inner Pt atoms for complexes **1**−**4**.

cations **1**−**4** (Figure 2). The frontier orbitals are essentially comparable to those from the EHMO calculations.[5e] For complex **1**, the HOMO is composed of a σ-bonding interaction between the hybridized d_σ orbitals of the terminal Pt atoms and the p_σ orbital of the central Pt atom, and the next LUMO (NLUMO) is derived from a σ-antibonding interaction between the hybridized d_σ orbitals of the terminal Pt atoms and the d_σ orbitals of the central Pt atom. Notably, the LUMO is a widely delocalized π-bonding orbital comprised of the p_π orbital of the central Pt atom, the hybridized p_π/d_π orbitals of the terminal Pt atoms, and the p_π orbitals of the isocyanide moieties (N≡C π^* orbitals). When the terminal xylyl isocyanides were replaced by MesNC (**2**) and *t*-BuNC (**4**), the corresponding three MOs are slightly destabilized with the increase of σ-donating ability of the isocyanide, and as a result, the relative energy levels between them did not largely change. In the calculations for **3**, atomic charge of the Pt ligated by XylNC is 0.01 and that by *t*-BuNC is −0.18, clearly demonstrating the presence of a π *trans* influcence of the terminal isocyanides. Although the MO calculations on complex **5** with *p*-TolNC ligands were not carried out since no plausible coordinates were obtained, some speculations can be made as follows. When the terminal XylNC ligands are replaced by *p*-TolNC, the interaction between the terminal platinum atoms and the isocyanide will be stronger owing to its decreased bulkiness. In this case, the HOMO and the NLUMO will be destabilized because both MOs involve σ-antibonding interactions between the platinum atoms and the isocyanide ligands. In contrast, the LUMO is estimated to be stabilized, since it involves π-bonding overlap between the Pt p_π/d_π and the RNC π^* orbitals. This speculation is in accord with the fact that the $\sigma\rightarrow\pi$ (HOMO−LUMO) electron transfer band is significantly shifted to lower energy in

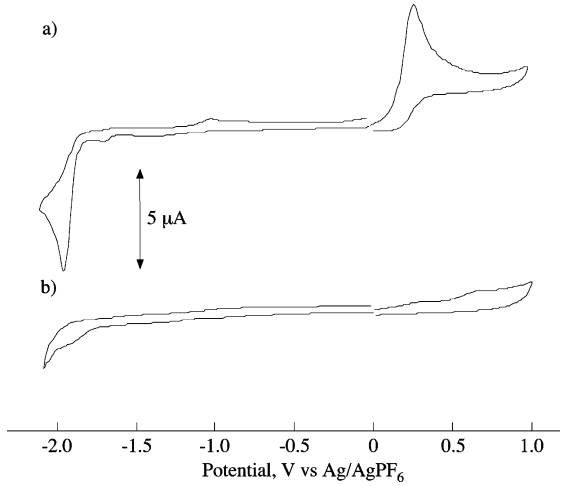

Figure 3. Cyclic voltammograms of (a) **1** and (b) **7a** in acetonitrile containing 0.1 M $[n\text{-}Bu_4N][PF_6]$ with a scan rate of 100 mV/s.

complex **5**, while the $\sigma\rightarrow\sigma^*$ (HOMO−NLUMO) transfer band is not.

(iii) Electrochemistry. The electrochemical properties of the linear triplatinum complexes **1**−**5** were analyzed by cyclic voltammetry. The cyclic voltammogram (CV) of **1** in acetonitrile showed an irreversible oxidation wave at 0.28 V (vs $Ag/AgPF_6$) and an irreversible reduction wave at −1.95 V, which corresponded to $[Pt_3]^{2+} \rightarrow [Pt_3]^{4+}$ and $[Pt_3]^{2+} \rightarrow [Pt_3]^0$ two-electron-transfer processes, respectively, on the basis of coulometric analyses (Figure 3). The CVs of **2** and **4** were almost identical to that of **1**; the oxidation and reduction waves were observed at 0.31 and −1.97 V for **2** and at 0.24 and −2.03 V for **4**. In the CV of **5**, the corresponding processes occurred at −0.20 and −1.93 V, which is consistent with the smaller HOMO−LUMO gap, and the unstable nature of complex **5** could be reflected on the lower potential for the oxidation.

Anion Exchange Reactions of $[Pt_3(\mu\text{-dpmp})_2(XylNC)_2](PF_6)_2$ (1). Reactions of complex **1** with excess KI, $Na[BPh_4]$, and $K_2[Pt(CN)_4]$ afforded the counteranion-exchanged complexes $[Pt_3(\mu\text{-dpmp})_2(XylNC)_2]X_2$ (X = I (**6a**), BPh_4 (**6b**), $1/2[Pt(CN)_4]$ (**6c**) (Scheme 1). The electronic spectra of **6a**−**6c** exhibited the characteristic absorption bands as observed in **1**. The ^1H and $^{31}P\{^1H\}$ NMR spectra also indicated the symmetrical linear triplatinum structure. However, the IR spectra of **6a** exhibited the presence of two kinds of terminal isocyanide ligands with ν(N≡C) 2139, 2109 cm^{-1} (**6a**). The detailed structures of **6a** and **6c** were determined by X-ray crystallography (Figures S5 and S6), and the structural parameters are listed in Table 6. While two Pt−Pt bond lengths of **1** are almost equal, at 2.723(2) and 2.724(2) Å, those found in **6a** are appreciably different, at 2.717(1) and 2.748(1) Å, the former being slightly shorter and the latter being quite longer than those in **1**. The considerable difference of the Pt−Pt bond distances (Δ = 0.031 Å) should be responsible for the two N≡C vibration energies, whereas meaningful differences between the two terminal isocyanides are not observed in the crystal structure. The two iodide anions are symmetrically arranged with the I···I vector vertical to the Pt−Pt−Pt axis, with distances between the central Pt atom and the I atoms of 6.803(2) and

Scheme 2

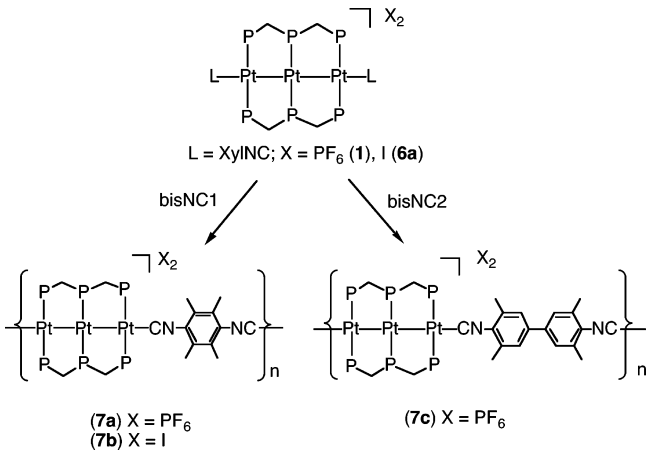

6.907(2) Å. In complex **6c**, the Pt−Pt bond lengths of 2.7696(7) and 2.7506(7) Å are remarkably longer than those of **1**, and all other bond lengths and angles concerning the isocyanides are usual. These structural features suggested that the elongation of the Pt−Pt bonds in **6c** did not result from the stronger interaction of the terminal Pt atoms with the isocyanide ligands as discussed above, and instead, it may be brought about by some electrostatic interaction with the counteranions in the lattice, although the detailed reasons are not clear. In the crystal packing, the triplatinum dications and the $[Pt(CN)_4]^{2-}$ anions are alternatively arranged, with the centers of the fragments separated at 7.6536(8) and 7.0158(7) Å. These results demonstrated that the Pt−Pt bond of the $\{Pt_3(\mu\text{-dpmp})_2L_2\}^{2+}$ unit, in the solid state, might be influenced by its counteranions.

Reactions of $[Pt_3(\mu\text{-dpmp})_2(XylNC)_2](PF_6)_2$ (1) with Bisisocyanides Affording Rigid-Rod Organometallic Polymers. On the basis of the terminal isocyanide exchange reactions as described above, π-conjugated bisisocyanides were used to construct rigid-rod organometallic polymers involving the linear triplatinum units. When a dichloromethane solution of **1** was carefully mixed with a dichloromethane solution containing ca. 2 equiv of the bulky bisisocyanide 2,3,5,6-tetramethylphenylene-1,4-bisisocyanide (bisNC1), an orange crystalline compound formulated as $\{[Pt_3(\mu\text{-dpmp})_2(bisNC1)](PF_6)_2\}_n$ (**7a**) was isolated in high yields (Scheme 2). When the ratio of bisNC1 was decreased to 1 and 0.5 equiv, the same compound was obtained although the yield was reduced. Complex **6a** also reacted with bisNC1 to afford orange crystals of the polymer compound $\{[Pt_3(\mu\text{-dpmp})_2(bisNC1)]I_2\}_n$ (**7b**). When **6b** and **6c** were used as starting material, no polymeric compound was isolated in pure form. Complex **1** in dichloromethane solution reacted with 2,2′,6,6′-tetramethyl-4,4′-bisphenylene-1,1′-bisisocyanide (bisNC2) to give orange microcrystals of the Pt_3 cluster polymer formulated as $\{[Pt_3(\mu\text{-dpmp})_2(bisNC2)](PF_6)_2\}_n$ (**7c**). Compounds **7a**−**7c** are sparingly soluble in MeCN and DMF and insoluble in most organic solvents such as CH_2Cl_2 and acetone.

The structure of compound **7a** was unambiguously determined by X-ray crystallography; an ORTEP plot for the polymer units and the crystal packing diagram are illustrated in Figures 4 and 5, and selected bond lengths and angles are listed in Table 8. The asymmetric unit contains the dicationic unit $\{Pt_3(\mu\text{-dpmp})_2(bisNC1)\}$, two hexafluorophosphate anions, and three dichloromethane solvent molecules. The linear triplatinum units, $\{Pt_3(\mu\text{-dpmp})_2\}^{2+}$ (Pt1−Pt2−Pt3 = 179.48(5)°), are covalently connected by the bisisocyanide ligands along the Pt−Pt−Pt axis (*b* axis) to construct a linearly ordered infinite-chain structure, $\{[Pt_3(\mu\text{-dpmp})_2(bisNC1)]^{2+}\}_n$, or a real rigid-rod, which is regarded as the first structurally characterized rigid-rod polymer involving linear organometallic cluster units. The structure of the Pt_3 unit is almost identical to that of complex **1**, which is supported by two dpmp ligands forming a C_2 symmetrical arrangement around the Pt_3 axis. The two C_2 chiral structures for the pair of dpmp ligands are involved in a single chain of complex **7a**, leading to a severely disordered structure of dpmp ligands which were refined by a two-site model with each having 0.5 occupancy (one set of dpmp ligands are drawn in Figures 4 and 5). It should be noted that these disordered features resulted in the low accuracy of the structural parameters. The metal−metal bond distances of Pt1−Pt2 = 2.7020(8) Å and Pt2−Pt3 = 2.6966(8) Å (av Pt−Pt = 2.6993 Å) are shorter by 0.025 Å than those found in **1**, indicating weaker π back-bonding interaction between the terminal Pt atoms and the bisisocyanide ligands. The N≡C groups of bisNC1 are linearly attached to the Pt_3 unit with av Pt−Pt−C = 176.6°, av Pt−C−N = 176°, and av C−N−C = 178°. The aromatic ring of bisNC1 is approximately vertical to the coordination plane of the terminal Pt atoms, due presumably to avoiding steric repulsion between the phenyl groups of dpmp and *o*-methyl groups of the bisNC1 ligands. In the crystal packing (Figure 5), the $\{[Pt_3(\mu\text{-dpmp})_2(bisNC)]^{2+}\}_n$ rigid-rods are assembled along the *b* axis and hexafluorophosphate anions are dispersed between the rods. The EXAFS analyses for **7a** and **7c** also indicated the linear Pt_3 structures with av Pt−Pt = 2.71(4) Å (**7a**) and 2.72(4) Å (**7c**) (Table 3 and Figure S3).

The ^1H and $^{31}P\{^1H\}$ NMR spectra in acetonitrile-d_3 exhibited spectral patterns comparable to those of **1** except some broadening features (Figure 6), implying that **7a** existed at least as oligomers in solution. Vapor pressure osmometric analysis of **7a** in acetonitrile indicated that the average formula weight is ca. 10 000−12 000 (n = ca. 5−6), although low accuracy should be considered owing to its low solubility. The electronic absorption spectrum of **7a** exhibited a slight but appreciable red-shift and broadening of the characteristic bands around 360−500 nm in comparison with that of **1** (Figure 7). Since the LUMO of the triplatinum complex **1** was shown to consist of a π-bonding interaction between the π^* orbital of the CN unit and the p_π/d_π hybridized orbital of the terminal Pt atom, an overlap of the LUMOs between the neighboring Pt_3 units may be responsible for the electronic absorption spectral features upon polymerization. The CV of **7a** showed an interesting result; that is, no electrochemical process was observed in the potential window in which complex **1** exhibited two-electron oxidation and reduction processes (Figure 3b). One can assume that the structural rigidness of **7a** prevented the electrochemical processes which may be accompanied by dynamic structural changes of the Pt_3 cores, or the large molecular size of

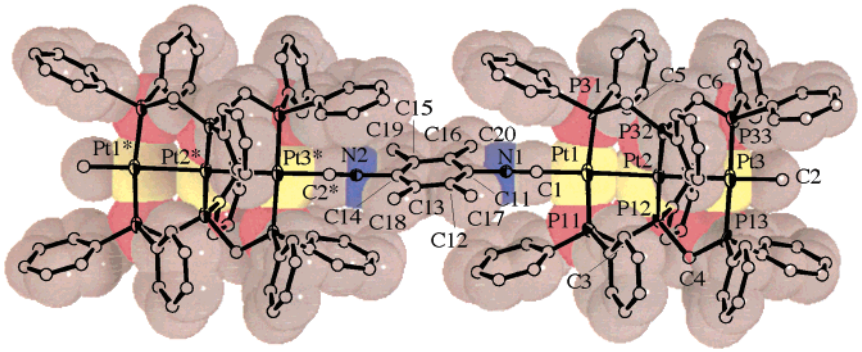

Figure 4. Perspective plot of the polymer units of **7a** with van der Waals radii superimposed with an ORTEP plot; Pt (yellow), P (red), N (blue), and C (gray). One set of the disordered dpmp ligands are drawn for clarity.

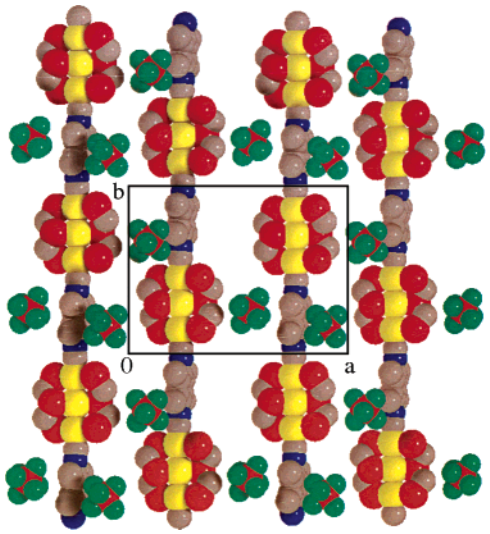

Figure 5. Crystal packing diagram of **7a** projected along the *c* axis with van der Waals radii. The phenyl rings are omitted for clarity; Pt (yellow), P (red), F (green), N (blue), and C (gray).

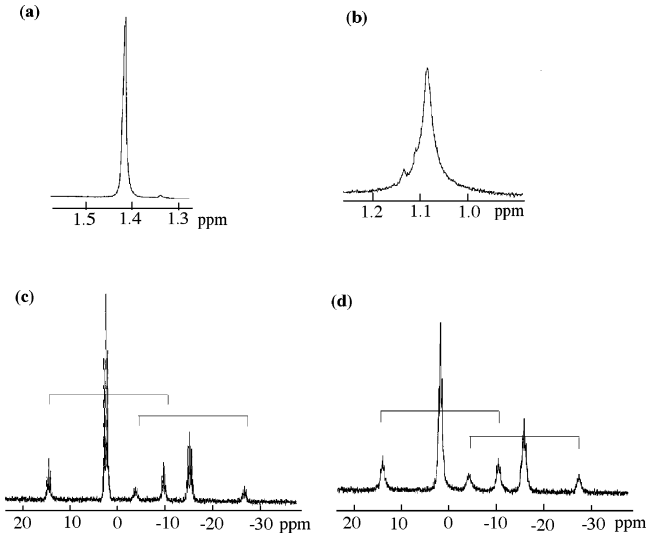

Figure 6. ^{1}H NMR spectra for the methyl protons of isocyanide ligands of (a) **1** in CD_2Cl_2 and (b) **7a** in CD_3CN at room temperature. $^{31}P\{^{1}H\}$ NMR spectra for the dpmp ligands of (c) **1** in CD_2Cl_2 and (d) **7a** in CD_3CN at room temperature.

Table 8. Selected Bond Lengths (Å) and Angles (deg) for Compound 7a

Bond Lengths			
Pt1−Pt2	2.7020(8)	Pt2−Pt3	2.6966(8)
Pt1−P11	2.217(7)	Pt1−P31	2.319(8)
Pt2−P12	2.271(8)	Pt2−P32	2.255(9)
Pt3−P13	2.313(8)	Pt3−P33	2.282(8)
Pt1−C1	1.93(2)	Pt3−C2	1.98(2)
N1−C1	1.16(3)	N2−C2*	1.02(2)
Bond Angles			
Pt1−Pt2−Pt3	179.48(5)	Pt2−Pt1−P11	85.3(2)
Pt2−Pt1−P31	85.8(2)	Pt2−Pt1−C1	176.7(9)
P11−Pt1−P31	170.6(3)	P11−Pt1−C1	93.5(7)
P31−Pt1−C1	95.2(7)	Pt1−Pt2−P12	90.7(2)
Pt1−Pt2−P32	92.4(2)	Pt3−Pt2−P12	89.1(2)
Pt3−Pt2−P32	87.8(2)	P12−Pt2−P32	176.9(3)
Pt2−Pt3−P13	88.6(2)	Pt2−Pt3−P33	89.7(2)
Pt2−Pt3−C2	176.5(8)	P13−Pt3−P33	177.2(4)
P13−Pt3−C2	92.4(6)	P33−Pt3−C2	89.2(6)
Pt1−C1−N1	173(3)	Pt3−C2−N2*	178(3)
C1−N1−C11	177(3)	C2*−N2−C14	178(2)

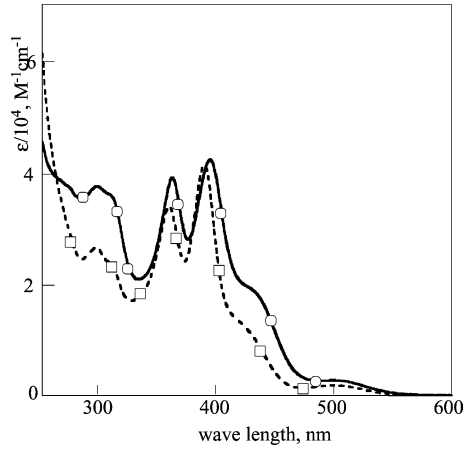

Figure 7. Electronic absorption spectra of **1** (—○—) and **7a** (···□···) in acetonitrile.

7a led to poor interaction with the surface of the working electrode.

Reactions of **1** with the less bulky bisisocyanides phenylene-1,4-bisisocyanide (bisNC3) and 2,5-dimethylphenylene-1,4-bisisocyanide (bisNC4) exclusively resulted in the formation of green powders formulated as $[(bisNCx)Pt_3(dpmp)_2(bisNCx)Pt_3(dpmp)_2(bisNCx)](PF_6)_4$ (x = 3 (**8a**), 4 (**8b**)) (Scheme 3). EXAFS analyses demonstrated that compounds **8a**,**b** involved the linear $\{Pt_3(\mu\text{-dpmp})_2\}$ cores with significantly longer Pt−Pt distances (2.85(4) Å (**8a**), 2.86(4) Å (**8b**)) (Table 7 and Figure S3), suggesting that an extensive migration of metal−metal bonding electrons into CN π^* orbitals resulted in the longer Pt−Pt distances. The contribution of structure **B** in Scheme 3 may prevent further polymerization by reducing σ-donating ability of the terminal,

Scheme 3

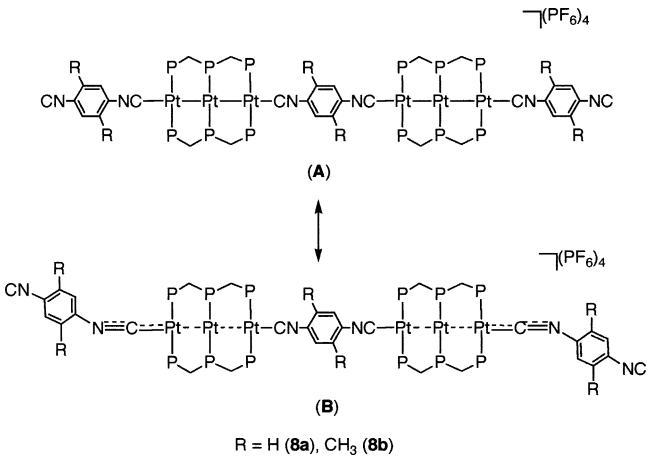

Scheme 4

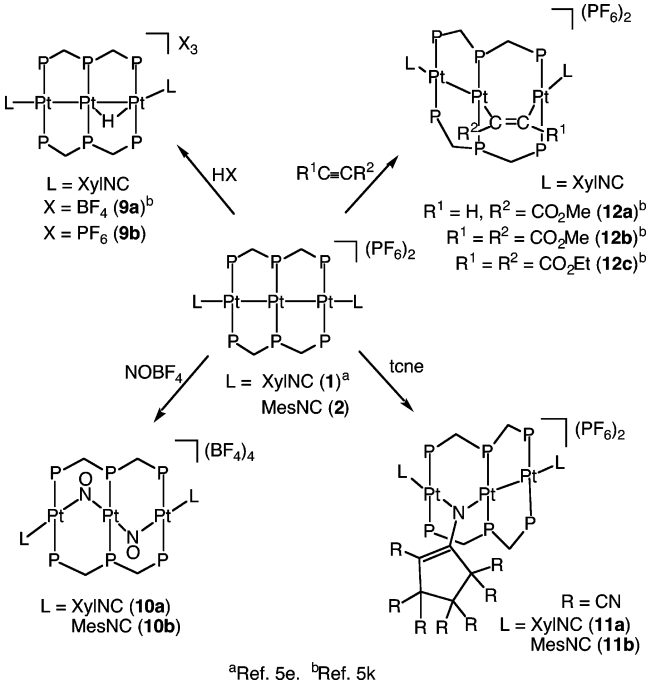

uncoordinated CN groups. A similar phenomenon was observed in *cis*-[W(dppe)$_2$(bisNC3)$_2$] (dppe = 1,2-bis(diphenylphosphino)ethane).[18] The poor solubility of compounds **8a**,**b** prevented further detailed characterization.

Reactions of [Pt$_3$(μ-dpmp)$_2$(XylNC)$_2$](PF$_6$)$_2$ (1) and Rigid-Rod Polymer {[Pt$_3$(μ-dpmp)$_2$(bisNC)](PF$_6$)$_2$}$_n$ (7a) with Small Ions and Organic Molecules. The linear triplatinum complex **1** possesses a widespread, coordinatively unsaturated plane comprised of the three platinum atoms with 44 valence electrons, and thus, we have studied the reactivity of **1** with electrophilic small ions and organic molecules. Complex **1** readily reacted with HBF_4 to be converted into the hydride-inserted asymmetric triplatinum complex [Pt$_3$(μ-H)(μ-dpmp)$_2$(XylNC)$_2$](BF$_4$)$_3$ (**9a**),[5k] and the reactions with electron-deficient alkynes afforded [Pt$_3$(μ-R^{1}C=CR^2)(μ-dpmp)$_2$(XylNC)$_2$](PF$_6$)$_2$ (**12a**, R^1 = H, R^2 = CO$_2$Me; **12b**, R^1 = R^2 = CO$_2$Me; **12c**, R^1 = R^2 = CO$_2$Et) (Scheme 4). The structure of **12a** was characterized by X-ray crystallography. Notably, even with a large excess of the reagents, only one Pt−Pt bond of the linear Pt$_3$ unit underwent the oxidative insertions. In the present study, to elucidate the detailed structure of [Pt$_3$(μ-H)(μ-dpmp)$_2$(XylNC)$_2$]$^{3+}$ (**9**), an X-ray crystallographic analysis for the analogous complex [Pt$_3$(μ-H)(μ-dpmp)$_2$(XylNC)$_2$](PF$_6$)$_3$ (**9b**) was performed. In addition, reactions of complex **1** with nitrosyl cation ($NOBF_4$) and tetracyanoethylene (tcne) were examined before the study of reactions on the polymer compound **7a**.

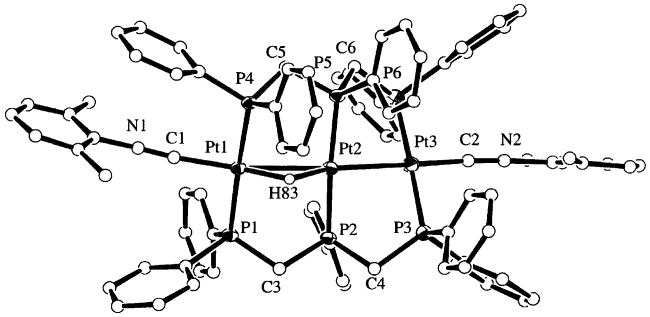

Figure 8. ORTEP plot of the complex cation of **9b**, [Pt$_3$(μ-H)(μ-dpmp)$_2$(XylNC)$_2$](BF$_4$)$_3$. The N and C atoms are drawn with arbitrary circles for clarity.

Table 9. Selected Bond Lengths (Å) and Angles (deg) for Compound 9b

Bond Lengths			
Pt1−Pt2	2.8680(6)	Pt2−Pt3	2.6374(6)
Pt1−P1	2.313(3)	Pt1−P4	2.318(3)
Pt2−P2	2.265(3)	Pt2−P5	2.272(3)
Pt3−P3	2.313(2)	Pt3−P6	2.305(3)
Pt1−C1	1.98(1)	Pt3−C2	1.88(2)
N1−C1	1.13(3)	N2−C2	1.12(2)
Pt1−H83	1.64	Pt2−H83	1.70
Bond Angles			
Pt1−Pt2−Pt3	171.49(2)	Pt2−Pt1−P1	89.33(7)
Pt2−Pt1−P4	89.22(7)	Pt2−Pt1−C1	160.3(3)
P1−Pt1−P4	176.56(9)	P1−Pt1−C1	91.4(3)
P4−Pt1−C1	91.1(3)	Pt1−Pt2−P2	93.61(7)
Pt1−Pt2−P5	92.04(7)	Pt3−Pt2−P2	86.25(8)
Pt3−Pt2−P5	87.22(8)	P2−Pt2−P5	171.5(1)
Pt2−Pt3−P3	88.62(8)	Pt2−Pt3−P6	90.75(8)
Pt2−Pt3−C2	178.6(5)	P3−Pt3−P6	177.6(1)
P3−Pt3−C2	92.4(5)	P6−Pt3−C2	88.2(5)
Pt1−C1−N1	174(1)	Pt3−C2−N2	171(1)
C1−N1−C11	166(1)	C2−N2−C21	178(1)
C1−Pt1−H83	168.0	Pt3−Pt2−H83	158.3
Pt2−Pt1−H83	31.4	Pt1−Pt2−H83	30.2
Pt1−H83−Pt2	118		

(i) Structure of [Pt$_3$(μ-H)(μ-dpmp)$_2$(XylNC)$_2$](PF$_6$)$_3$ (9b). An ORTEP plot for the complex cation of **9b** is given in Figure 8, and selected bond distances and angles are listed in Table 9. The complex cation **9b** is composed of a triplatinum core that is bridged by two dpmp ligands and is terminally capped by two isocyanide molecules. The linear arrangement of the three Pt atoms is deformed from linearity with a Pt1−Pt2−Pt3 angle of 171.49(2)°. The Pt2−Pt3 distance of 2.6374(6) Å demonstrated that the Pt−Pt bond was retained; however, the Pt1−Pt2 distance of 2.8680(6) Å is significantly longer than those observed in **1** (av 2.724 Å) and is not a value for normal Pt−Pt single bonds. The hydrogen atom (H83) was found by difference Fourier synthesis to sit between the Pt1 and Pt2 atoms and bind to the terminal Pt1 atom with Pt1−H83 = 1.64 Å and to the central Pt2 atom with Pt2−H83 = 1.70 Å. The

(18) Wagner, N. L.; Laib, F. E.; Bennett, D. W. *J. Am. Chem. Soc.* **2000**, *122*, 10856.

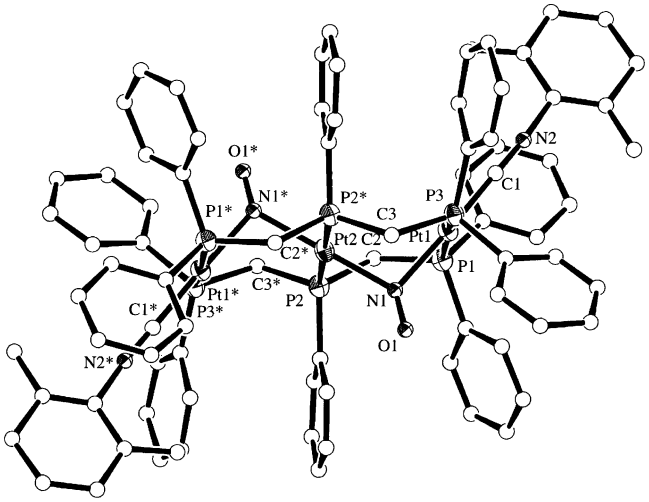

Figure 9. ORTEP plot of the complex cation of **10a**, $[Pt_3(\mu\text{-NO})_2(\mu\text{-dpmp})_2(XylNC)_2](BF_4)_4$. The O, N, and C atoms are drawn with arbitrary circles for clarity.

Table 10. Selected Bond Lengths (Å) and Angles (deg) for Compound 10a

Bond Lengths			
Pt1···Pt2	3.0962(4)	Pt1−P1	2.358(2)
Pt1−P3	2.343(2)	Pt1−N1	2.020(6)
Pt1−C1	1.923(8)	Pt2−P2	2.321(2)
Pt2−N1	2.019(6)	O1−N1	1.09(1)
N2−C1	1.14(1)		
Bond Angles			
P1−Pt1−P3	171.47(7)	P1−Pt1−N1	86.6(2)
P1−Pt1−C1	90.4(2)	P3−Pt1−N1	87.0(2)
P3−Pt1−C1	96.3(2)	N1−Pt1−C1	176.1(2)
P2−Pt2−P2*	180.0	P2−Pt2−N1	87.1(2)
P2*-Pt2−N1	92.9(2)	N1−Pt2−N1*	180.0
Pt1−N1−Pt2	100.1(3)	Pt1−N1−O1	125.9(6)
Pt2−N1−O1	133.2(6)	Pt1−C1−N2	175.7(7)
C1−N2−C11	172.7(7)		

Pt1−H83−Pt2 angle is 118°. The terminal isocyanide attached to Pt1 is tilted from a collinear position with Pt2−Pt1−C1 = 160.3(3)° and is arranged in a *trans* position to the H83 atom with C1−Pt1−H83 = 168.0°. These structural features revealed that a H^+ was readily trapped in one of the Pt−Pt bonds to form the $Pt_2(\mu\text{-H})$ unit with a three-center/two-electron interaction and cause a slight deformation of the linear triplatinum structure.

(ii) Reactions of Complexes 1 and 2 with $NOBF_4$. When complex **1** was treated with an excess of $NOBF_4$ at room temperature, pale green crystals of $[Pt_3(\mu\text{-dpmp})_2(\mu\text{-NO})_2(XylNC)_2](BF_4)_4$ (**10a**) were isolated in good yield. Similar reaction of **2** also gave $[Pt_3(\mu\text{-dpmp})_2(\mu\text{-NO})_2(MesNC)_2](BF_4)_4$ (**10b**). The IR spectra of **10a**,**b** indicated the presence of terminal isocyanide ligands around 2200 cm^{-1} and nitrosyl units at about 1510 cm^{-1}, the latter corresponding to the values for a N−O triple bond rather than a double bond. The structure of **10a** was determined by X-ray crystallography. An ORTEP plot for the complex cation is shown in Figure 9, and selected bond lengths and angles are listed in Table 10. The complex cation has a crystallographically imposed inversion center on the central platinum (Pt2) and consists of three platinum atoms bridged by two dpmp ligands. The Pt−Pt separation of 3.0962(4) Å suggested the absence of a Pt−Pt bond. The Pt−Pt distance in **10a** is shorter than those for the A-frame diplatinum complexes with dppm ligands, e.g., $[Pt_2Cl_2(\mu\text{-NO})(\mu\text{-dppm})_2](BPh_4)$ (3.246 Å),[19a] $[Pt_2Cl_2(\mu\text{-NO})(\mu\text{-dppm})_2](BF_4)$ (3.186 Å),[19b] $[Pt_2Cl_2(\mu\text{-CH}_2)(\mu\text{-dppm})_2]$ (3.151 Å),[20] and is comparable to that of $[Pt_2Cl_2(\mu\text{-CS}_2)(\mu\text{-dppm})_2]$ (3.094 Å).[21] Two nitrosyl groups are inserted into the two Pt−Pt bonds of **10a** with an almost symmetrical manner, resulting in a double-A-frame trimetallic structure. The N−O bond length of 1.09(1) Å corresponds to values for neutral N−O triple bonds rather than N−O double bonds[22] and is in agreement with the IR data. This nitrosyl-bridged structure is quite different from that of $[Pt_2Cl_2(\mu\text{-NO})(\mu\text{-dppm})_2]^+$, which involves an NO^- unit with an N−O bond length of 1.20(2) Å.[19,20] The present reaction can be regarded as a three-center oxidative addition proceeding on a linear triplatinum center, which involves an apparent two-electron transfer from the triplatinum core to two NO^+ ions.

Structurally characterized nitrosyl-bridged diplatinum complexes are extremely rare, probably owing to the low-lying LUMO and small HOMO−LUMO gap as Hoffmann predicted theoretically on the basis of extended Hückel MO calculations.[23] EHMO calculations on a model compound **C**, $[Pt_3(\mu\text{-NO})_2(PH_3)_6(CNH)_2]^{4+}$ (C_i), along with fragment analysis with the fragments $[Pt_3(PH_3)_6(CNH)_2]^{2+}$ (**C1**) and $[(NO)_2]^{2+}$ (**C2**) suggested some reasons why the stable, nitrosyl-inserted complex was isolated (Figure S7). The triplatinum system **C1** has a Pt−Pt σ-bonding orbital (HOMO) and a σ-antibonding orbital (LUMO) at higher and lower energy levels, respectively, than the corresponding σ_{Pt-Pt} and σ^*_{Pt-Pt} orbitals of the diplatinum model. The decrease of the $\sigma-\sigma^*$ energy gap causes the HOMO and LUMO of **C1** to be well matched with the low-lying π^* orbitals of **C2**, generating two significant bonding interactions (3u and 5g MOs of **C** in Figure S7). These two bonding orbitals should be responsible for partial electron transfer from the Pt_3^{2+} core to the two bridging NO^+ groups and stabilizes the double-A-frame structure.

(iii) Reactions of Complexes 1 and 2 with Tetracyanoethylene. When complex **1** or **2** was treated with an excess of tetracyanoethylene (tcne) in CH_2Cl_2, the color of the solution immediately changed from orange to pale green, resulting in the formation of $[Pt_3(\mu\text{-}C_{12}N_8)(\mu\text{-dpmp})_2(RNC)_2](PF_6)_2$ (R = Xyl (**11a**), Mes (**11b**)). The detailed structure of **11a** was determined by X-ray crystallographic analysis (Figure 10 and Table 11). The complex cation involves an asymmetrical triplatinum core supported by two dpmp ligands and capped by two isocyanide molecules. The Pt1−Pt2 distance of 2.6446(8) Å corresponds to a Pt−Pt single bond, and the Pt2−Pt3 separation of 3.2150(8) is indicative of no Pt−Pt bonding interaction. The two tcne molecules were coupled to form a (heptacyanocyclopent-1-enyl)nitrene moiety, which was inserted into one of the Pt−Pt bonds of **1**. Structurally characterized nitrene-bridged platinum and palladium complexes are

(19) (a) Neve, F.; Ghedini, M.; Tirpicchio, A.; Ugozzoli, F. *Organometallics* **1992**, *11*, 795. (b) Ghedini, M.; Neve, F.; Mealli, C.; Tirpicchio, A.; Ugozzoli, F. *Inorg. Chim. Acta* **1990**, *178*, 5.
(20) Azam, K. A.; Frew, A. A.; Lloyd, B. R.; Manojlovic-Muir, L.; Muir, K. W.; Puddephatt, R. J. *Organometallics* **1985**, *4*, 1400.
(21) Cameron, T. S.; Gardner, P. A.; Grundy, K. R. *J. Organomet. Chem.* **1981**, *212*, C19.
(22) Enemark, J. H.; Feltham, R. D. *Coord. Chem. Rev.* **1974**, *13*, 339.
(23) Hoffman, D. M.; Hoffmann, R. *Inorg. Chem.* **1981**, *20*, 3543.

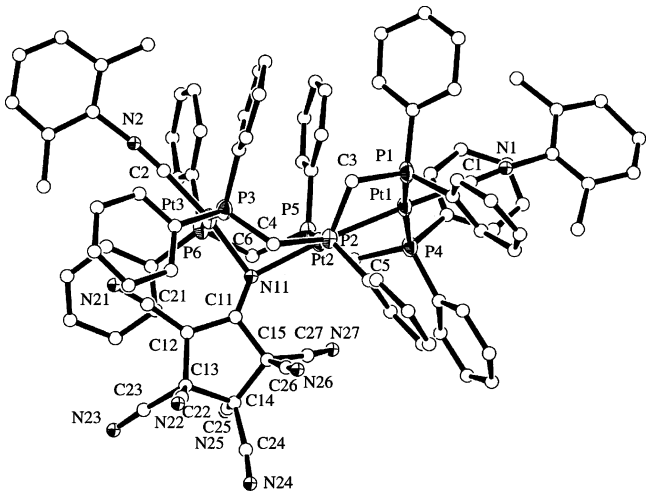

Figure 10. ORTEP plot of the complex cation of **11a**, $[Pt_3(\mu\text{-}C_{12}N_8)(\mu\text{-dpmp})_2(XylNC)_2](PF_6)_2$. The N and C atoms are drawn with arbitrary circles for clarity.

Table 11. Selected Bond Lengths (Å) and Angles (deg) for Compound 11a

Bond Lengths			
Pt1−Pt2	2.6446(8)	Pt2···Pt3	3.2150(8)
Pt1−P1	2.312(5)	Pt1−P4	2.328(5)
Pt2−P2	2.263(4)	Pt2−P5	2.277(4)
Pt3−P3	2.341(4)	Pt3−P6	2.349(4)
Pt1−C1	2.01(2)	Pt3−C2	1.90(2)
Pt2−N11	2.18(1)	Pt3−N11	2.05(1)
N1−C1	1.11(3)	N2−C2	1.16(2)
N11−C11	1.26(2)	N21−C21	1.10(2)
N22−C22	1.14(3)	N23−C23	1.13(4)
N24−C24	1.09(3)	N25−C25	1.11(3)
N26−C26	1.11(3)	N27−C27	1.05(3)
C11−C12	1.46(2)	C11−C15	1.54(2)
C12−C13	1.54(3)	C13−C14	1.60(3)
C14−C15	1.57(3)		
Bond Angles			
Pt2−Pt1−P1	93.9(1)	Pt2−Pt1−P4	88.9(1)
Pt2−Pt1−C1	177.8(6)	P1−Pt1−P4	173.4(2)
P1−Pt1−C1	87.4(5)	P4−Pt1−C1	89.6(5)
Pt1−Pt2−P2	89.5(1)	Pt1−Pt2−P5	87.3(1)
Pt1−Pt2−N11	175.1(4)	P2−Pt2−P5	169.6(2)
P2−Pt2−N11	92.2(4)	P5−Pt2−N11	91.8(4)
Pt3−Pt2−P5	87.22(8)	P2−Pt2−P5	171.5(1)
P3−Pt3−P6	174.9(1)	P3−Pt3−N11	89.3(4)
P3−Pt3−C2	91.8(6)	P6−Pt3−N11	87.3(4)
P6−Pt3−C2	92.0(6)	N11−Pt3−C2	173.0(6)
Pt1−C1−N1	173(2)	Pt3−C2−N2	174(1)
C1−N1−C31	174(2)	C2−N2−C41	175(2)
Pt2−N11−Pt3	98.9(6)	Pt2−N11−C11	138(1)
Pt3−N11−C11	123(1)	N11−C11−C12	129(2)
N11−C11−C15	123(2)	C12−C11−C15	108(1)
C11−C12−C13	110(1)	C12−C13−C14	103(2)
C13−C14−C15	102(2)	C11−C15−C14	105(1)

extremely rare.[24] The N11 atom asymmetrically bridges Pt2 and Pt3 and adopts a planar sp^2 geometry. The Pt_2N plane is almost coplanar with the [C11C12] olefin unit and the relatively shorter N11−C11 bond length (1.26(2) Å), indicating that the electron density on the N atom is delocalized through p_π−p_π interaction between the

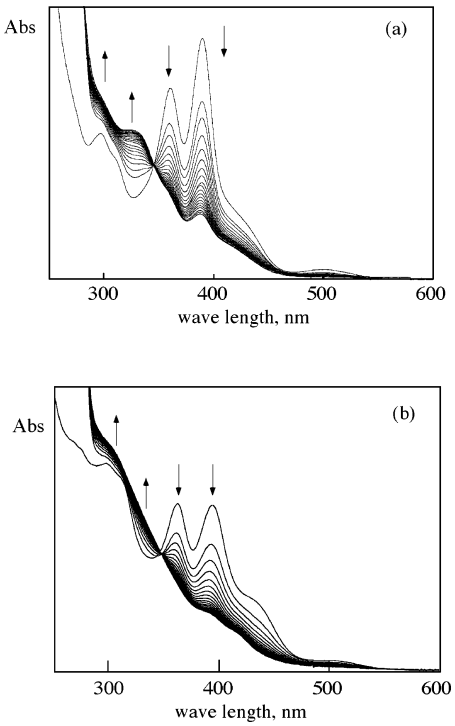

Figure 11. Electronic absorption spectral changes for (a) reaction of **1** with tcne (10 equiv) in dichloromethane (monitored every 30 s) and (b) reaction of **7a** with tcne (10 equiv) in acetonitrile (monitored every 4 min).

nitrene and the olefin units. In accordance with this, the C11−C12 bond length (1.46(2) Å) is longer than the values of usual C−C double bonds. A similar tendency was observed in $[Ir_2(CO)_2(\mu\text{-dppm})_2(\mu\text{-NPh})]$[25] and $[Rh_2(CO)_2(dppm)_2(\mu\text{-N}(p\text{-}NO_2C_6H_4))]$[26] (dppm = bis(diphenylphosphino)methane). The heptacyanocyclopent-1-enyl moiety takes an envelope conformation with the C14 atom in the apex site and the C13, C14, and C15 atoms having an sp^3 tetrahedral configuration. The present type of tcne cyclic dimerization is very rare, and the related compound has been reported only as *N*-(heptacyanocyclopent-1-enyl)triphenylphosphoranimine, which was formed by reaction of tcne with triphenylphosphine.[27] The reaction of **1** with an excess of tcne in dichloromethane was monitored by electronic absorption spectral change with an isosbestic point at 345 nm (Figure 11a), showing first-order dependency on the starting complex **1** with the pseudo-first-order rate constant of 4.0×10^{-3} s^{-1}. When complex **1** was treated with 1 equiv of tcne, complex **11a** was isolated as the sole product in low yields. Although no stable intermediate was identified, one of the plausible mechanisms is depicted in Scheme 5. At the initial step, the tcne adduct (**D1**) was assumed to be formed by analogy with reaction of **1** with electron-deficient alkynes.[5k] The strong *trans* influence of the Pt−Pt bond may cause the zwitterionic Pt−C bond breaking (**D2**), and the nucleophilic attack of the carbanion on the electron-deficient nitrile carbon of the second tcne molecule (**D3**) was inferred as a key step for the coupling. The similar cyclic

(24) (a) Besenyei, G.; Párkányi, L.; Foch, I.; Simándi, L. I.; Kálmán, A. *Chem. Commun.* **1997**, 1143. (b) Lee, S. W.; Trogler, W. C. *Inorg. Chem.* **1990**, *29*, 1099. (c) Jones, R.; Kelly, P. K.; Williams, D. J.; Woollins, J. D. *Chem. Commun.* **1985**, 1325. (d) Kelly, P. F.; Slawin, A. M. Z.; Williams, D. J.; Woollins, J. D. *Polyhedron* **1990**, *9*, 1567. (e) Meij, R.; Stufkens, D. J.; Vrieze, K.; Brouwers, A. M. F.; Overbeek, A. R. *J. Organomet. Chem.* **1978**, *155*, 123. (f) Foch, I.; Párkányi, L.; Besenyei, G.; Simándi, L. I.; Kálmán, A. *J. Chem. Soc., Dalton Trans.* **1999**, 293. (g) Leung, W.-H.; Chim, J. L. C.; Wong, W.-T. *J. Chem. Soc., Dalton Trans.* **1997**, 3277.

(25) Ye, C.; Sharp, P. R. *Inorg. Chem.* **1995**, *34*, 55.

(26) Ge, Y.-W.; Peng, F.; Sharp, P. R. *J. Am. Chem. Soc.* **1990**, *112*, 2632.

(27) (a) Mohan, T.; Day, R. O.; Holmes, R. R. *Inorg. Chem.* **1992**, *31*, 2271. (b) Butterfield, P. J.; Tebby, J. C.; King, T. J. *J. Chem. Soc., Perkin Trans. 1* **1978**, 1237.

Scheme 5

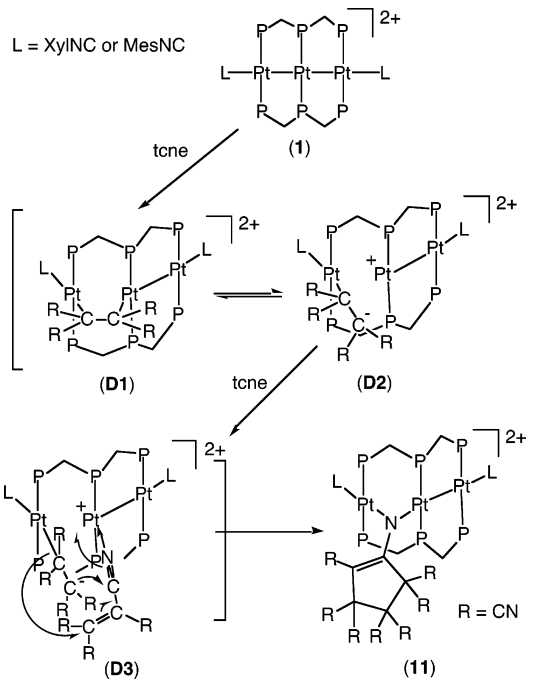

Scheme 6

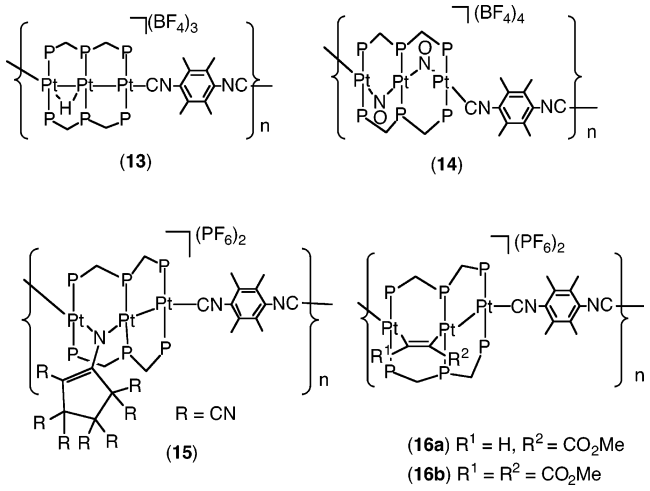

dimerization was not observed with other electron-deficient olefins such as RHC═CHR (R = CN, CO_2CH_3). It should be noted that the diplatinum complex $[Pt_2(\mu\text{-dppm})_2(XylNC)_2](PF_6)_2$[28] did not promote the cyclic dimerization of tcne.

(iv) Reactions of Polymer 7a with Small Ions and Molecules. The cluster polymer **7a** was proven to be remarkably reactive with H^+, NO^+, tcne, and electron-deficient acetylenes even in heterogeneous systems with CH_3CN and/or CH_2Cl_2. When a suspension of **7a** in CH_2Cl_2 was treated with an excess of HBF_4, the yellow polymeric compound $\{[Pt_3(\mu\text{-H})(\mu\text{-dpmp})_2(bisNC1)](BF_4)_3\}_n$ (**13**) was obtained in good yield (Scheme 6). The IR and UV−vis spectroscopic data were similar to those of $[Pt_3(\mu\text{-H})(\mu\text{-dpmp})_2(XylNC)_2](BF_4)_3$ (**9a**), except some broadening features (Figure S8). In light of the crystal structure of **9b**, the cluster polymer **13** was estimated to have a slightly undulating polymeric structure. When the yellow polymer **13** was treated with an excess of Et_3N in dichloromethane, the orange rigid-rod polymer **7** (counteranion should be BF_4^-) was regenerated. The electronic absorption spectrum in acetonitrile was closely similar to that of **7a** (Figure S8).

Treatment of a suspension of **7a** in acetonitrile/dichloromethane with excess of $NOBF_4$, tcne, and $R^1C{\equiv}CR^2$ (R^1 = $COOCH_3$, H; R^2 = $COOCH_3$) afforded the polymers formulated as $\{[Pt_3(\mu\text{-NO})_2(\mu\text{-dpmp})_2(bisNC1)](BF_4)_4\}_n$ (**14**), $\{[Pt_3(\mu\text{-}C_{12}N_8)(\mu\text{-dpmp})_2(bisNC1)](PF_6)_2\}_n$ (**15**), and $\{[Pt_3(\mu\text{-}R^1C{=}CR^2)(\mu\text{-dpmp})_2(bisNC1)](PF_6)_2\}_n$ (**16a**, R^1 = H, R^2 = $COOCH_3$; **16b**, R^1 = R^2 = $COOCH_3$), respectively, which were characterized by elemental analysis, IR, and UV−vis spectroscopy (Scheme 6). The spectra of **14**−**16** were similar to those of the corresponding complexes **10**−**12** except for some broadening features. In the case of tcne, the reaction was monitored by electronic absorption spectral change with an isosbestic point at 348 nm in acetonitrile (Figure 11b). The reaction of polymer **7a** with the pseudo-first-order rate constant of 7.0×10^{-4} s^{-1} proceeded considerably slower than that of **1** (4.3×10^{-3} s^{-1} in CH_3CN). In light of the crystal structures of $[Pt_3(\mu\text{-NO})_2(\mu\text{-dpmp})_2(XylNC)_2](BF_4)_4$ (**10a**), $[Pt_3(\mu\text{-}C_{12}N_8)(\mu\text{-dpmp})_2(XylNC)_2](PF_6)_2$ (**11a**), and $[Pt_3(\mu\text{-HC}{=}CCO_2CH_3)(\mu\text{-dpmp})_2(XylNC)_2](PF_6)_2$ (**12a**),[5k] the polymers of **14**−**16** were estimated to have zigzag structures. The present reactions could be developed by a method by which some functional pendant groups are incorporated into the linear organometallic polymer **7a**.

Conclusion

In this study, it was found that the axial 2,6-xylyl isocyanide ligands of the linear triplatinum complex $[Pt_3(\mu\text{-dpmp})_2(XylNC)_2](PF_6)_2$ (**1**) were replaced by other isocyanide molecules, and the structure and properties of the Pt_3 core could be tuned by varying the substituents of the isocyanide ligands. By utilizing the axial ligand exchange reactions with π-conjugated bulky bisisocyanides, rigid-rod organometallic polymers including the linear triplatinum units $\{[Pt_3(\mu\text{-dpmp})_2(bisNC)](PF_6)_2\}_n$ (bisNC = 2,3,5,6-tetramethylphenylene-1,4-bisisocyanide (**7a**), 2,2′,6,6′-tetramethyl-4,4′-bisphenylene-1,1′-bisisocyanide (**7c**)) were successfully synthesized and characterized in detail. Furthermore, the polymer **7a** was revealed to be readily reactive with electrophiles, H^+, NO^+, tcne, and electron-deficient alkynes, to afford small molecules/ions inserted within zigzag polymers. The present results could provide a useful strategy for molecular-based functional materials in which linearly ordered multimetallic centers are incorporated.

Acknowledgment. This work was partly supported by a Grant-in-Aid for Scientific Research from the Ministry of Education, Culture, Sports, Science, and Technology of Japan.

Supporting Information Available: Tabulation of X-ray crystallographic data, including experimental details, atomic parameters, bond distances and angles, and ORTEP plots of complexes **2, 4**, **6a**, and **6c**. The results of EXAFS analyses for compounds **1**, **2**, **4**, **5**, **7a**, **7c**, **8a**, and **8b**. The electronic absorption spectra of complexes **1**−**5**. The MO interaction diagram for the model complex **10**. The electronic absorption spectra of **13** and of **13** with Et_3N. This material is available free of charge via the Internet at http://pubs.acs.org.

OM0494566

(28) Yamamoto, Y.; Yamazaki, H. *Organometallics* **1993**, *12*, 933.